EUROPEAN ORGANIZATION FOR NUCLEAR RESEARCH (CERN)

CERN-EP-2026-116
2026/10/12

CMS-HIG-24-002

Search for a new heavy scalar resonance decaying to a pair of Z bosons in the four-lepton final state in proton-proton collisions at $\sqrt{s} = 13$ TeV

The CMS Collaboration*

arXiv:2605.26462v2 [hep-ex] 8 Oct 2026

Abstract

A search for a new heavy scalar resonance decaying to two Z bosons, each subsequently decaying to a pair of electrons or muons, is presented. The results are based on a proton-proton collision data set collected by the CMS experiment at the LHC at a center-of-mass energy of 13 TeV, corresponding to an integrated luminosity of 138 fb^{-1}. The search is performed over a wide range of resonance masses from 130 GeV to 3 TeV, considering both narrow- and broad-width scenarios, and considering the gluon fusion and vector boson fusion production processes. For the broad-width scenario, the interference between the new resonance, the 125 GeV Higgs boson production, and the continuum background is taken into account. No significant excess with respect to the standard model background expectation is observed in the examined phase space. Upper limits at the 95% confidence level are set on the product of the heavy scalar resonance production cross section and the branching fraction for its decay into two Z bosons. The exclusion limits range from 0.05–0.1 pb in the low-mass region to 0.005 pb in the high-mass region.

Published in the Journal of High Energy Physics as doi:10.1007/JHEP10(2026)006.

© 2026 CERN for the benefit of the CMS Collaboration. CC-BY-4.0 license

*See Appendix A for the list of collaboration members

1 Introduction

In 2012, the ATLAS and CMS Collaborations discovered a boson [1–3] with a mass close to 125 GeV and with properties consistent with those expected for the Higgs boson (H) predicted by the standard model of particle physics (SM). This discovery represents a major breakthrough for the field of particle physics and a significant validation of the SM, which postulates the existence of this particle as an excitation of the Higgs field.

The SM, however, presents several limitations. For example, it does not include a description of gravity or dark matter and does not explain the origin of the matter-antimatter asymmetry in the universe. These issues could be addressed by a range of theories beyond the SM (BSM). In many models describing such BSM effects, additional scalar resonances are predicted, e.g., additional Higgs bosons in two-Higgs doublet models [4] and radions in models with warped extra dimensions [5–7].

Previous searches for a new boson decaying to a pair of Z bosons have been performed by the CMS [8, 9] and ATLAS [10, 11] Collaborations using proton-proton collision data collected in Run 1 (2011–2012) and Run 2 (2015–2018) of the CERN LHC. In these searches, no evidence for a signal was observed.

In this paper, a search for a heavy scalar resonance X is presented in the decay channel $X \to ZZ \to 4\ell$ where the leptons ℓ are electrons (e) or muons (μ). Since the mass of the new resonance is not known, the search is performed over a wide mass range from 130 GeV to 3 TeV. The resonance can be produced via gluon fusion (ggF) or vector boson fusion (VBF). Compared with the previous CMS search at 13 TeV [9], which used the 2016 data set corresponding to an integrated luminosity of 35.9 fb^{-1}, this analysis uses the full Run 2 data set of 138 fb^{-1}. It also benefits from the final Run 2 reprocessing, which incorporates improved detector alignment, calibrations, and reconstruction conditions, as well as updated lepton identification and jet flavor tagging algorithms. The numerical results are provided in HEPData [12].

2 The CMS detector

The CMS apparatus [13, 14] is a multipurpose, nearly hermetic detector, designed to trigger on [15–17] and identify electrons, muons, photons, and charged and neutral hadrons [18–20]. Its central feature is a superconducting solenoid of 6 m internal diameter, providing a magnetic field of 3.8 T. Within the solenoid volume are a silicon pixel and strip tracker, a lead tungstate crystal electromagnetic calorimeter (ECAL), and a brass and scintillator hadron calorimeter (HCAL), each composed of a barrel and two endcap sections. Forward calorimeters extend the pseudorapidity (η) coverage provided by the barrel and endcap detectors. Muons are reconstructed using gas-ionization detectors interleaved with the layers of the steel flux-return yoke outside the solenoid. More detailed descriptions of the CMS detector, together with a definition of the coordinate system used and the relevant kinematic variables, can be found in Refs. [13, 14].

Events of interest are selected using a two-tiered trigger system. The first level (L1), composed of custom hardware processors, uses information from the calorimeters and muon detectors to select events at a rate of around 100 kHz within a fixed latency of 4 μs [15]. The second level, known as the high-level trigger, consists of a farm of processors running a version of the full event reconstruction software optimized for fast processing and reduces the event rate to a few kHz before data storage [16, 17].

3 Data and simulated samples

The search is performed using the pp collision data set collected by the CMS experiment in 2016–2018 [21–23], with a total integrated luminosity of 138 fb^{-1}.

Events are selected by the online trigger system before undergoing the reconstruction described in Section 4. The online selection is based on dielectron, dimuon, and electron-muon trigger algorithms. Additional triggers, requiring three leptons with low transverse momentum (p_{T}) thresholds and no isolation criteria, as well as single-lepton triggers, are also used to increase the selection efficiency. The applied p_{T} thresholds range from 20 to 25 GeV for single-lepton triggers, from 8 to 23 GeV for double-lepton triggers, and from 5 to 16 GeV for triple-lepton triggers.

The trigger efficiency measurement follows the strategy adopted in Ref. [24], using a "tag-and-probe" method [25]. The efficiency is greater than 99% in most of the phase space and is compatible between the observed data and simulation within statistical uncertainties.

Monte Carlo (MC) simulated samples are used to model the signal, background, and interference processes.

Samples of X resonances produced via ggF or VBF are generated at next-to-leading order (NLO) in perturbative quantum chromodynamics (pQCD) with the POWHEG 2.0 [26–28] generator. Their decays into two Z bosons and then into four leptons are modeled with JHUGEN 7.0.2 [29–32], including corrections for the ZZ branching fraction and angular correlations among the fermions. Samples are generated for a wide range of masses of the X resonance (m_{X}), from 125 GeV to 3 TeV, with the width (Γ_{X}) set to the values predicted by the complex pole scheme [33, 34] for $m_{\mathrm{X}} < 1$ TeV. For those with $m_{\mathrm{X}} > 1$ TeV, the width cannot be predicted by this scheme, and is therefore set conventionally to $0.5 m_{\mathrm{X}}$. However, the search is performed using a range of width assumptions, not restricted to the widths in the simulated samples. These samples are used to derive models for signal processes, as well as for 125 GeV Higgs boson production.

Events in ggF production samples generated with POWHEG are weighted to take advantage of predictions at next-to-NLO (NNLO) accuracy in pQCD, matched to a parton shower [35] (NNLOPS). These weights are obtained from the ratio of the production cross section at NNLOPS accuracy to the production cross section obtained with the POWHEG event generator. The weights are applied as a function of the number of jets and the p_{T} of the resonance at the generator level.

The dominant background process originates from the production of two Z bosons from quark-antiquark annihilation $\mathrm{q\bar{q}} \to \mathrm{ZZ} \to 4\ell$, also referred to as qqZZ, which is simulated at NLO in pQCD with POWHEG. The differential production cross section as a function of the invariant mass of the two Z bosons m_{ZZ} has been computed at NNLO in pQCD, but it is not yet available in a parton-level event generator. Therefore, the NNLO/NLO correction factor (K factor) for the qqZZ background, ranging from 1 to 1.25, is applied to the POWHEG sample as a function of m_{ZZ} [36]. Additional NLO electroweak corrections depending on the initial-state quark flavor and kinematic properties are applied to the qqZZ background process, ranging from 0.7 to 1.

Another important background is the loop-induced production of two Z bosons through gluon fusion $\mathrm{gg} \to \mathrm{ZZ} \to 4\ell$, also referred to as ggZZ, which is generated at leading order (LO) with MCFM 7.0 [37–39]. The LO-to-NNLO K factor computed for $\mathrm{gg} \to \mathrm{H} \to \mathrm{ZZ}$ is used to reweight the simulated samples of ggZZ events, as the K factors for these two processes have been shown to be compatible by several theoretical calculations [40–42].

The K factor is computed as a function of m_{ZZ} using the HNNLO v2 program [43–45], ranging from 2 to 2.6.

The background of $qq \to qqZZ$ via t-channel, u-channel, or quartic interactions is also generated at LO with MCFM 7.0. It is referred to as VBFZZ in what follows. Samples of triboson events (WWZ, WZZ) are simulated at NLO in pQCD using MADGRAPH5_aMC@NLO 2.6.5 [46], and the backgrounds from the production of top quarks associated with vector bosons ($t\bar{t}Z$, $t\bar{t}ZZ$, $t\bar{t}WW$) are generated at LO using MADGRAPH5_aMC@NLO.

Additional samples of WZ, Drell–Yan, and top quark-antiquark pair ($t\bar{t}$) production are used in the estimation of reducible backgrounds (described in Section 8.2). The first two processes are simulated using MADGRAPH5_aMC@NLO at NLO in pQCD, whereas the latter is generated at NLO in pQCD with POWHEG [47].

Additionally, samples combining the Higgs boson production, interfering background processes and interference are generated at LO with MCFM 7.0, considering both the ggF and VBF production mechanisms. These samples are used to study the interference between signal and background processes. The matrix element likelihood approach (MELA) [29–31, 48] is used to compute likelihoods using the topologies of events and matrix elements (MEs) of various processes. Based on this calculation, weights are computed to be applied to events in the samples to model the interference contributions.

All simulated samples are interfaced with PYTHIA 8.230 [49] to simulate parton showering and hadronization effects, with the CP5 tune [50] used to model the underlying event. The NNPDF 3.1 [51] parton distribution functions (PDFs) are used in the generation of events. The response of the CMS detector is modeled with GEANT4 [52]. The simulated events are reconstructed with the same algorithms as used for data. Pileup (PU), the presence of additional pp interactions in the same or nearby bunch crossings, is simulated with PYTHIA and added to all events. The simulated samples are corrected such that their PU distribution matches the distribution observed in data.

4 Event reconstruction and selection

The particle-flow (PF) algorithm [53] is used to reconstruct and identify individual particles in the event with an optimized combination of the raw information from each subdetector. The reconstructed particles are referred to as PF candidates. The energy of photons is measured in the ECAL. Electrons are reconstructed by associating the reconstructed tracks in the inner tracker with the ECAL clusters, the latter additionally considering the bremsstrahlung photon showers geometrically compatible with the electron track. The electron energy is obtained from the combination of the track momentum at the primary vertex (PV) and the cluster energy, where the PV is taken to be the vertex corresponding to the hardest scattering in the event, evaluated using tracking information alone, as described in Ref. [54]. The muon momentum is measured from the track momenta in both the inner tracker and the muon detectors. The energy of charged hadrons is determined by combining tracks in the inner tracker with the associated energy deposits in both the ECAL and HCAL, with corrections to take into account the imperfect linear energy response of calorimeters. Finally, the energy of neutral hadrons is determined from the energy deposits in the ECAL and HCAL.

Electrons with transverse momenta $p_T^e > 7\,\text{GeV}$ are reconstructed within the detector acceptance region, corresponding to a pseudorapidity range of $|\eta^e| < 2.5$ [18]. For each electron, the impact parameter significance, defined as the ratio of the three-dimensional (3D) impact

parameter with respect to the PV to its uncertainty, is required to be < 4. This ensures the suppression of nonprompt leptons from hadron decays or photon conversions. Electrons are identified using a boosted decision tree algorithm based on the XGBOOST framework [55], including electron isolation information. The algorithm was developed for the analysis in Ref. [24], with an updated training performed for Ref. [56].

Muons with $p_{\mathrm{T}}^{\mu} > 5\,\mathrm{GeV}$ are reconstructed within the detector acceptance region $|\eta^{\mu}| < 2.4$, combining the information from the silicon tracker and the muon system [19]. The same impact parameter requirements as for electrons are applied. Cases where tracks in the tracker are matched to hits in only one or two muon planes are used to recover very low p_{T} muons that do not traverse the entire detector. The muons considered in this analysis are selected from the muon track candidates by applying loose requirements on the track in the muon system and the inner tracker. For muons with $p_{\mathrm{T}}^{\mu} > 200\,\mathrm{GeV}$, dedicated identification requirements are applied to improve the efficiency [19].

To distinguish the muon candidates from the Z boson decay from those from hadronic decays within jets, a requirement on the relative isolation $\mathcal{I}^{\mu} < 0.35$ is imposed, which was optimized in Ref. [57]. The relative isolation is defined as:

$$\mathcal{I}^{\mu} = \frac{1}{p_{\mathrm{T}}^{\mu}} \left(\sum_{\substack{\text{charged} \\ \text{hadrons}}} p_{\mathrm{T}} + \max \left[\left(\sum_{\substack{\text{neutral} \\ \text{hadrons}}} p_{\mathrm{T}} + \sum_{\text{photons}} p_{\mathrm{T}} - \frac{1}{2} \sum_{\substack{\text{charged} \\ \text{hadrons}}} p_{\mathrm{T}}^{\mathrm{PU}} \right), \, 0\,\mathrm{GeV} \right] \right) \tag{1}$$

where the sums are performed over PF candidates i within a cone of $\Delta R(\mu, i) < 0.3$, with $\Delta R(\mu, i) = \sqrt{(\eta^{\mu} - \eta^{i})^2 + (\phi^{\mu} - \phi^{i})^2}$, where ϕ is the azimuthal angle in radians. The first sum involves charged hadrons originating from the PV, and the second term involves neutral hadrons and photons. The contribution of neutral particles from PU vertices, estimated as half the contribution of charged hadrons from PU, is subtracted. The total contribution from neutral particles is guaranteed to be non-negative by the max function.

Photons originating through final-state radiation (FSR) from the selected leptons are recovered to improve the accuracy of the Z boson candidate mass reconstruction. Particle-flow photons satisfying $p_{\mathrm{T}}^{\gamma} > 2\,\mathrm{GeV}$, $|\eta^{\gamma}| < 2.4$, and relative isolation $\mathcal{I}^{\gamma} < 1.8$ are considered as FSR candidates. This selection was optimized in Ref. [2]. Each candidate is associated to the closest lepton in the event and is required to have $\Delta R(\gamma, \ell)/E_{\mathrm{T},\gamma}^2 < 0.012/\,\mathrm{GeV}^2$ and $\Delta R(\gamma, \ell) < 0.5$, where $E_{\mathrm{T},\gamma}$ is the transverse energy of the photon. For each lepton, only the photon with the lowest $\Delta R(\gamma, \ell)/E_{\mathrm{T},\gamma}^2$ is retained. The FSR candidates are excluded from the computation of the muon isolation.

Lepton reconstruction and selection efficiencies are measured with a tag-and-probe method, selecting Z boson decays both in data and in simulation, separately for electrons and muons in bins of p_{T} and η. All MC samples are corrected by the ratio of the efficiency in data to that in simulation. The lepton energy scale and resolution are calibrated using known resonances decaying to two leptons in bins of p_{T} and η. Detailed descriptions of this calibration are given in Refs. [18, 19].

Hadronic jets are clustered from PF candidates using the infrared- and collinear-safe anti-k_{T} algorithm [58] with a distance parameter of 0.4. The jet energy is computed from the vectorial sum of all PF candidates clustered inside it. Since the reconstructed jet energy is on average 5–10% larger than the true jet energy in simulation, particles from PU vertices are discarded from the jet composition, and residual corrections are applied. The corrections are derived from dijet, γ + jets, Z + jets, and multijet events [59]. In this analysis, hadronic jets are required

to have $p_T^{jet} > 30\,GeV$ and $|\eta^{jet}| < 4.7$. Requirements are made on their energy fractions of different types of particles, and they must have $\Delta R > 0.4$ with respect to all selected leptons and associated photons. For jets with $p_T^{jet} < 50\,GeV$, a dedicated identification algorithm is used to reject jets from PU [60].

The jet flavor is identified using the DEEPCSV algorithm [61–63], a deep neural network based algorithm to tag heavy-flavor jets. Jets that pass the working point with a 68% tagging efficiency for b jets, a 10–20% mistagging probability for c jets, and a 1% mistagging probability for light flavor jets are considered to be b tagged. Since most jets from VBF stem from light-flavor quarks, vetoing b-tagged jets suppresses backgrounds containing b jets and improves the sensitivity to the VBF production process.

The described PF objects are used as input to the event selection, which targets events with at least four identified and isolated leptons originating from the PV. The event selection follows that employed in Ref. [24] and is summarized below.

Pairs of leptons with opposite charge and same flavor, whose invariant mass must be $12 < m_Z < 120\,GeV$, are used to build Z boson candidates. Then, ZZ candidates are formed by selecting two of the Z boson candidates. The Z boson candidate with invariant mass closest to the nominal Z boson mass $m_Z^{nom} = 91.1876\,GeV$ [64] is defined as Z_1, and the other is defined as Z_2. Three mutually exclusive final states are defined on the basis of the flavors of the four leptons in the event: 4μ, 4e, and $2e2\mu$. The ZZ candidates must satisfy the following requirements:

- Any two of the four leptons must have $\Delta R(\ell_1, \ell_2) > 0.02$ to avoid reconstructed leptons overlapping.
- The Z_1 is required to have $m_{Z_1} > 40\,GeV$ to select the on-shell Z boson.
- Among the four leptons, the one with the highest (second highest) p_T must have $p_T > 20\,(10)\,GeV$, to ensure high trigger and reconstruction efficiency.
- Every pair of oppositely charged leptons among the four selected leptons, regardless of flavor, must have $m_{\ell^+\ell^-} > 4\,GeV$, to suppress QCD multijet events.
- In the 4μ and 4e final states, background processes containing a Z boson and a low-mass resonance such as J/ψ can pass the above selections by swapping one lepton between the two resonances. To avoid selecting such events, given a ZZ candidate, two alternative Z boson candidates are built by swapping the two positively charged leptons. The alternative Z boson candidate with the invariant mass closer to m_Z^{nom} is denoted as Z_a, the other as Z_b. The ZZ candidate is discarded if $|m_{Z_a} - m_Z^{nom}| < |m_{Z_1} - m_Z^{nom}|$ and $m_{Z_b} < 12\,GeV$.
- The invariant mass of the ZZ candidate is required to be greater than 70 GeV.

The signal region is composed of all events with at least one ZZ candidate, potentially with additional leptons. If more than one ZZ candidate satisfies the selection, the candidate with the highest value of a discriminant to distinguish signal and background processes, which will be defined in Section 5, is selected.

5 Observables

A new resonance would appear as a peak in the distribution of the reconstructed four-lepton mass $m_{4\ell}^{reco}$. The detector mass resolution at 125 GeV is around 1 GeV, reaching about 30, 60, and 90 GeV in the 4e, $2e2\mu$, and 4μ final states at a mass of 3 TeV, respectively. This is mainly because the electron energy resolution worsens at high energies due to shower containment and ECAL

calibration limitations, while the muon momentum resolution degrades more strongly due to reduced track curvature and increased sensitivity to alignment effects.

The left panel of Fig. 1 shows the $m_{4\ell}^{\text{reco}}$ distributions for various signal hypotheses, the background processes, and the observed data. All signal and background distributions are estimated from MC simulation, except the background involving jets misidentified as leptons, labelled Z + jets, which is estimated from data using the method described in Section 8.2. The remaining backgrounds include triboson production (WZZ, WWZ) and $t\bar{t}$ associated with vector bosons ($t\bar{t}Z$, $t\bar{t}ZZ$, $t\bar{t}WW$), which are collectively referred to as "other" backgrounds.

Signal processes with different masses and produced via different production mechanisms are shown, normalized to the Higgs boson production cross section expected in the SM. The various signal processes present a narrow peak for low masses, and can be prominent above backgrounds if they have sufficiently large production cross sections. The width of the distribution increases at higher resonance masses, as expected for SM-like Higgs bosons. At 3 TeV, the ggF signal is more prominent at low $m_{4\ell}^{\text{reco}}$ than the VBF signal, mostly because the gluon PDF decreases more rapidly than the quark PDF at high momentum fractions.

In addition to $m_{4\ell}^{\text{reco}}$, a kinematic discriminant $D_{\text{bkg}}^{\text{kin}}$ is considered to distinguish signal and background processes. This observable is computed using MELA, and is defined as a function of the likelihood ratios:

$$D_{\text{bkg}}^{\text{kin}} = \left[1 + \frac{\mathcal{P}_{\text{bkg}}^{q\bar{q}}\left(\vec{\Omega}^{H\to 4\ell} | m_{4\ell}^{\text{reco}}\right)}{\mathcal{P}_{\text{sig}}^{gg}\left(\vec{\Omega}^{H\to 4\ell} | m_{4\ell}^{\text{reco}}\right)} \right]^{-1} . \tag{2}$$

In this equation, $\mathcal{P}_{\text{bkg}}^{q\bar{q}}$ corresponds to the likelihood that the event originated from $q\bar{q} \to 4\ell$ and is calculated using the MEs from MCFM; $\mathcal{P}_{\text{sig}}^{gg}$ is calculated with the MEs from JHUGEN and defines the likelihood that the event originated from the production of a scalar resonance via ggF; and $\vec{\Omega}^{H\to 4\ell}$ refers to the angular phase space of the 4ℓ system plus the masses of the two Z bosons. They are computed as the probabilities of $\vec{\Omega}^{H\to 4\ell}$ conditional on $m_{4\ell}^{\text{reco}}$.

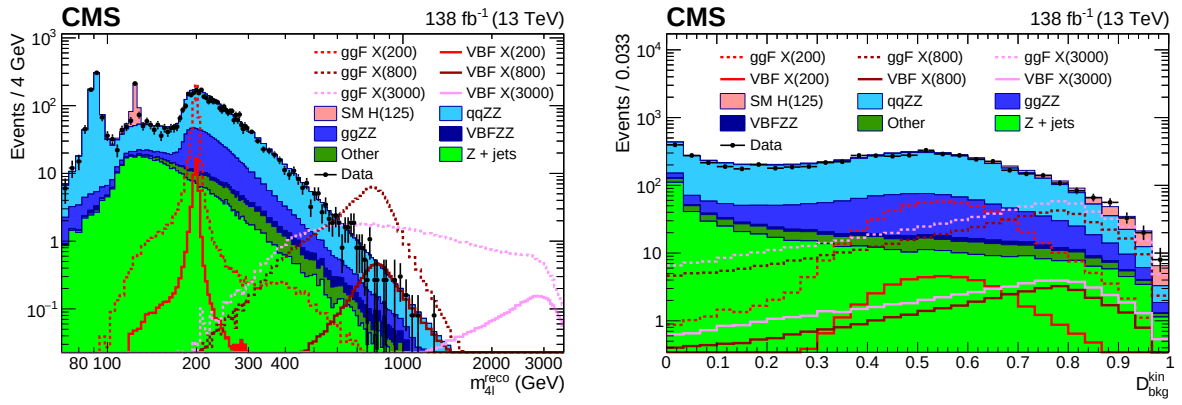


Figure 1: Left: the $m_{4\ell}^{\text{reco}}$ distributions for signal and background processes estimated from the MC simulation, alongside observed data. Red and pink open histograms show the lineshapes for different signal masses. Right: The $D_{\text{bkg}}^{\text{kin}}$ distributions for signal and background processes estimated from the MC simulation, together with the observed data. The masses of the X resonances written in the legends are in GeV units. The widths are 1.43 GeV for $m_X = 200$ GeV, 304 GeV for $m_X = 800$ GeV, and 1.5 TeV for $m_X = 3$ TeV [33].

The $D_{\text{bkg}}^{\text{kin}}$ distributions are illustrated in Fig. 1 (right) for several signal hypotheses alongside

background processes and the observed data. The backgrounds are mainly distributed around 0 and 0.5, whereas the signals are concentrated around 0.8, except for $m_X = 200\,\text{GeV}$, for which the distribution is concentrated around 0.5. This is because a resonance with $m_X = 200\,\text{GeV}$ has kinematical properties that are similar to the ZZ background, which has two on-shell Z bosons with $m_{4\ell}^{\text{reco}}$ distributed around 200 GeV. Apart from a small m_X range around 200 GeV, $D_{\text{bkg}}^{\text{kin}}$ is a powerful tool to discriminate signals at different masses against the background.

The observables $m_{4\ell}^{\text{reco}}$ and $D_{\text{bkg}}^{\text{kin}}$ are used to build two-dimensional (2D) templates, which allow us to distinguish between signal and background processes in the likelihood fit.

6 Event categorization

To improve the sensitivity of the analysis to the VBF production process, VBF-enriched regions are defined using the topology of the hadronic jets. The criteria used to categorize events are the same as those used in Ref. [9]. Two mutually exclusive categories are defined: the VBF-tagged one, containing events satisfying the criteria described below, and the untagged one, containing the remaining events, which are primarily produced via ggF.

The VBF tagging criteria include the following requirements, as a VBF signal event typically contains one or two reconstructed energetic jets, which are not likely to be b jets:

- There is no additional electron or muon that satisfies the lepton selection discussed in Section 4 in the event.
- There must be at least two jets that satisfy the jet selection described in Section 4.
- If there are two or three jets that satisfy the jet selection requirements, the number of b-tagged jets must be ≤ 1; otherwise, there must be no b-tagged jets in the event. This condition is a compromise between rejecting the $\text{t}\bar{\text{t}}$ background which usually contains b jets and retaining VBF signals that contain light jets mistagged as b jets.

Requirements are also placed on the discriminant $D_{\text{2jet}}^{\text{VBF}}$, computed with MELA and defined as:

$$D_{\text{2jet}}^{\text{VBF}} = \left[1 + \frac{\mathcal{P}_{\text{HJJ}}\left(\vec{\Omega}^{\text{H+JJ}} | m_{4\ell}^{\text{reco}}\right)}{\mathcal{P}_{\text{VBF}}\left(\vec{\Omega}^{\text{H+JJ}} | m_{4\ell}^{\text{reco}}\right)}\right]^{-1}, \tag{3}$$

where $\mathcal{P}_{\text{HJJ}}$ is the probability for the event topology to be similar to that of an SM Higgs boson produced via ggF in association with two jets, and $\mathcal{P}_{\text{VBF}}$ is the probability for the event topology to correspond to that of an SM Higgs boson produced via VBF. The angular phase space of the 4ℓ system and the two most energetic jets is denoted as $\vec{\Omega}^{\text{H+JJ}}$. These probabilities are calculated using JHUGEN MEs. Similar to $D_{\text{bkg}}^{\text{kin}}$, $D_{\text{2jet}}^{\text{VBF}}$ is defined conditional on the four-lepton mass.

Figure 2 shows the $D_{\text{2jet}}^{\text{VBF}}$ distributions of signal and background processes. Both the ggF signal and the background processes are distributed around 0, whereas the VBF signal processes are distributed around 1. For the VBF signals, a small fraction of events is distributed around 0: these correspond to the case where the two most energetic jets are not the two VBF jets but mostly ISR or FSR jets.

To be selected in the VBF-tagged category, events are required to have $D_{\text{2jet}}^{\text{VBF}} > 0.46$. This threshold maximizes the overall sensitivity to the VBF signal, taking into account the different mass hypotheses.

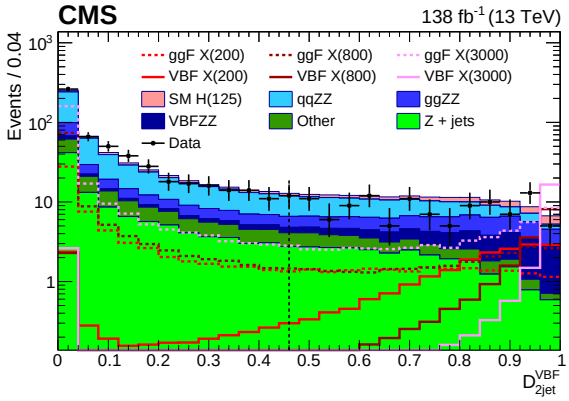


Figure 2: The $D_{\text{2jet}}^{\text{VBF}}$ distributions for signal, background, and observed data. Only events passing the lepton and jet multiplicity requirements for the VBF-tagged category are shown. The dotted vertical line represents the threshold of $D_{\text{2jet}}^{\text{VBF}} = 0.46$.

7 Signal modeling

To test a large number of signal hypotheses without simulating all of them, a parametric approach is used to model the different signals. The approach introduced in Ref. [9] is followed.

The signal model is constructed from parameterized signal templates obtained using MC simulation. Given the mass m_{X} and decay width Γ_{X} of the resonance, the probability density function (pdf) of the signal process is defined as

$$\mathcal{P}_{\text{sig}}(m_{4\ell}^{\text{reco}}, D_{\text{bkg}}^{\text{kin}}|m_{\text{X}}, \Gamma_{\text{X}}) = \{[\mathcal{M}(m_{4\ell}^{\text{gen}}|m_{\text{X}}, \Gamma_{\text{X}})\epsilon(m_{4\ell}^{\text{gen}})] \otimes \mathcal{R}(m_{4\ell}^{\text{reco}}|m_{4\ell}^{\text{gen}})\}\mathcal{P}(D_{\text{bkg}}^{\text{kin}}|m_{4\ell}^{\text{reco}}). \quad (4)$$

We have:

- The $\otimes$ denotes a convolution.
- The $\mathcal{M}(m_{4\ell}^{\text{gen}}|m_{\text{X}}, \Gamma_{\text{X}})$ describes the theoretical lineshape of the signal, with $m_{4\ell}^{\text{gen}}$ being the 4ℓ invariant mass at generator level.
- The $\epsilon(m_{4\ell}^{\text{gen}})$ is the overall signal efficiency, which accounts for the probability of the signal to fall within the detector acceptance, as well as the reconstruction, selection, and categorization efficiencies.
- The $\mathcal{R}(m_{4\ell}^{\text{reco}}|m_{4\ell}^{\text{gen}})$ is the signal resolution function, which converts the distribution from generator level to detector level, to account for the finite energy resolution of the detector.
- The $\mathcal{P}(D_{\text{bkg}}^{\text{kin}}|m_{4\ell}^{\text{reco}})$ is the template of $D_{\text{bkg}}^{\text{kin}}$ in bins of $m_{4\ell}^{\text{reco}}$, extending the formula to two dimensions.

The theoretical lineshape of the signal can be described as the differential production cross section as a function of $m_{4\ell}^{\text{gen}}$, and is based on Refs. [33, 65]. It is parameterized as

$$\mathcal{M}(m_{4\ell}^{\text{gen}}|m_{\text{X}}, \Gamma_{\text{X}}) = \sigma(m_{4\ell}^{\text{gen}}) \frac{2m_{\text{X}} m_{4\ell}^{\text{gen}} \Gamma_{\text{X}}}{[(m_{4\ell}^{\text{gen}})^2 - m_{\text{X}}^2]^2 + m_{\text{X}}^2 \Gamma_{\text{X}}^2}. \quad (5)$$

The spin-0 propagator is described by the Breit–Wigner function; the other factors contributing to the production cross section, including the proton PDFs, the MEs, and the kinematic phase space, are incorporated as a function of $m_{4\ell}^{\text{gen}}$ in $\sigma(m_{4\ell}^{\text{gen}})$, which is calculated with the MCFM

generator [37–39]. Such a parameterization has been confirmed to give the same lineshape as that directly generated by MCFM [9].

The signal efficiency $\epsilon(m_{4\ell}^{\text{gen}})$ is defined as the number of events within the detector acceptance, satisfying the online and offline selections, and falling in a certain category, divided by the total number of generated events. The efficiency is computed for each final state, data-taking period, and production mechanism. It is estimated from MC simulation as a function of $m_{4\ell}^{\text{gen}}$, and parameterized with an empirical function that is the product of a polynomial function and an error function. The χ^2 divided by the number of degrees of freedom of the fits is in the range 0.6–1.3. Figure 3 shows the signal efficiency evaluated from simulation for the 2018 data-taking period. In general, the efficiency is higher in the final states with muons. Signal processes have an overall efficiency of 14–80%. More than 90% of ggF signal events are categorized into the untagged category. For VBF signal events, as the mass grows, the fraction of VBF-tagged events decreases. This is because the two VBF jets tend to be less energetic at higher masses, as most of the energy of the partons is needed to produce the heavy resonance. The signal efficiencies are similar for the other data-taking periods.

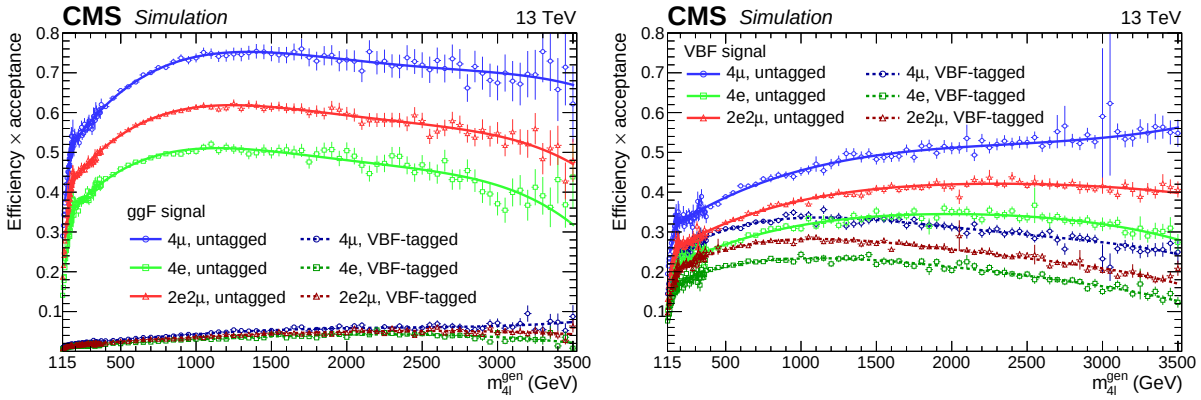


Figure 3: The product of signal efficiency and acceptance, as a function of $m_{4\ell}^{\text{gen}}$, computed for the 2018 data set. The left panel shows the results for ggF signals, and the right panel shows those for VBF signals. The points are values computed from simulation, which are fitted with the corresponding curves. In each panel, the product of efficiency and acceptance for each final state and category is shown: green squares and curves represent the 4e final state, red rectangles and curves indicate the 2e2μ final state, and blue circles and curves the 4μ final state; the solid lines with lighter colors represent the untagged category, and the efficiencies for the VBF-tagged categories are shown in dashed lines with darker colors.

The signal resolution $\mathcal{R}(m_{4\ell}^{\text{reco}}|m_{4\ell}^{\text{gen}})$ is described by a double Crystal Ball (DCB) function of $\Delta m_{4\ell} = m_{4\ell}^{\text{reco}} - m_{4\ell}^{\text{gen}}$ defined as

$$\text{DCB}(\Delta m_{4\ell}|\mu_{\text{res}},\sigma_{\text{res}},\alpha_1,n_1,\alpha_2,n_2) = \begin{cases} \left(\frac{n_1}{|\alpha_1|}\right)^{n_1} e^{-\frac{\alpha_1^2}{2}} \left(\frac{n_1}{|\alpha_1|} - |\alpha_1| - \frac{\Delta m_{4\ell}-\mu_{\text{res}}}{\sigma_{\text{res}}}\right)^{-n_1}, & \frac{\Delta m_{4\ell}-\mu_{\text{res}}}{\sigma_{\text{res}}} \leq -\alpha_1 \\ e^{-\frac{(\Delta m_{4\ell}-\mu_{\text{res}})^2}{2\sigma_{\text{res}}^2}}, & -\alpha_1 < \frac{\Delta m_{4\ell}-\mu_{\text{res}}}{\sigma_{\text{res}}} < \alpha_2 \\ \left(\frac{n_2}{|\alpha_2|}\right)^{n_2} e^{-\frac{\alpha_2^2}{2}} \left(\frac{n_2}{|\alpha_2|} - |\alpha_2| + \frac{\Delta m_{4\ell}-\mu_{\text{res}}}{\sigma_{\text{res}}}\right)^{-n_2}, & \frac{\Delta m_{4\ell}-\mu_{\text{res}}}{\sigma_{\text{res}}} \geq \alpha_2 \end{cases} \tag{6}$$

where all parameters $\mu_{\text{res}},\sigma_{\text{res}},\alpha_1,n_1,\alpha_2,n_2$ are dependent on $m_{4\ell}^{\text{gen}}$, with "res" denoting "resolution".

To compute the dependence on $m_{4\ell}^{\text{gen}}$, all signal samples are merged with equal normalization and divided into different $m_{4\ell}^{\text{gen}}$ bins. The distribution of $\Delta m_{4\ell}$ is then extracted and fitted with the DCB function to obtain the values of the six function parameters. The dependence of each parameter p on $m_{4\ell}^{\text{gen}}$ is fitted with the following function:

$$f_p(x) = a_{p,0} + a_{p,0.5}x^{0.5} + a_{p,1}x + a_{p,1.5}x^{1.5} + a_{p,2}x^2 + a_{p,2.5}x^{2.5}, \tag{7}$$

where $x = m_{4\ell}^{\text{gen}}$, $p = \mu_{\text{res}}, \sigma_{\text{res}}, \alpha_1, n_1, \alpha_2, n_2$. Several functional forms were studied, including polynomial functions and functions with the same form but a different order. Among these functions, f_p was found to have the best fit performance with stable convergence and without evident overfitting effects. A simultaneous fit is then performed over all $m_{4\ell}^{\text{gen}}$ bins, taking the $a_{p,i}$ as the parameters to be fitted. The method is applied individually for each production mechanism, in each final state, and for each data-taking period.

Following the above steps, the parametric model is built as a function of $m_{4\ell}^{\text{reco}}$. Examples are shown in Fig. 4, with various mass and width assumptions, for the two considered signal production mechanisms. The integral of each shape is normalized to 1. For $\Gamma_X = 4$ MeV, $m_{4\ell}^{\text{reco}}$ is mostly distributed around m_X; when the width is large, a large fraction of off-shell production is expected, especially for the signals with $m_X = 130$ and 3 TeV.

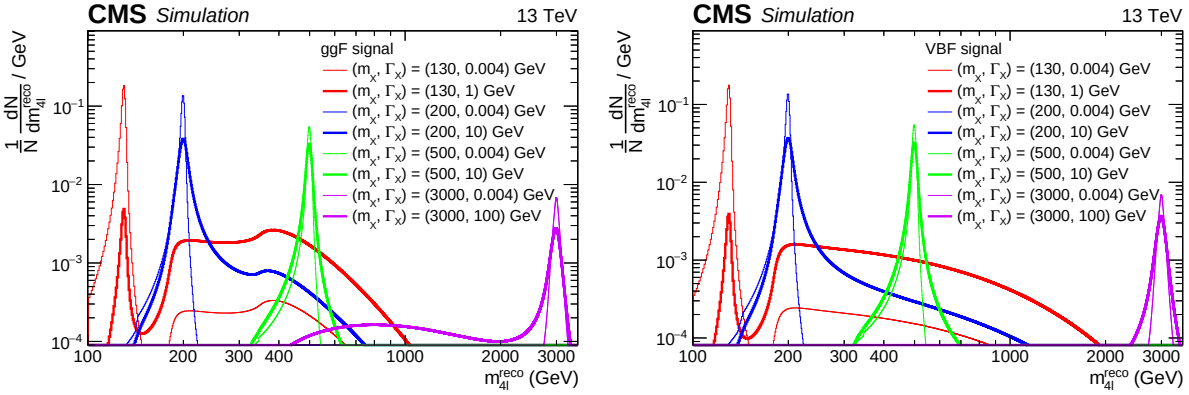


Figure 4: The $m_{4\ell}^{\text{reco}}$ distributions for several values of m_X and Γ_X obtained from the signal model, for the ggF (left) and VBF (right) signal processes. All final states and categories are combined.

To build the 2D pdf, the conditional pdf $\mathcal{P}(D_{\text{bkg}}^{\text{kin}}|m_{4\ell}^{\text{reco}})$ is obtained from the $m_{4\ell}^{\text{reco}}$ versus $D_{\text{bkg}}^{\text{kin}}$ distribution extracted from the signal MC simulation. Figure 5 shows examples of the distributions, for the two production mechanisms, in the 4μ final state. In each $m_{4\ell}^{\text{reco}}$ bin, the distribution is normalized to unity. The distributions are similar for the two production mechanisms, since $D_{\text{bkg}}^{\text{kin}}$ only depends on the kinematic properties of the 4ℓ final state.

The signal model is validated by comparing it with the $m_{4\ell}^{\text{reco}}$ distribution extracted from the MC simulation. In general, they are compatible within statistical fluctuations, except in the tails of the $m_{4\ell}^{\text{reco}}$ distribution for signals at $m_X > 500$ GeV, which show discrepancies around 2–10%. This is understood to be rooted in the difference between MCFM, which generates $\sigma(m_{4\ell}^{\text{gen}})$ in Eq. (5), and POWHEG, with which the simulation is performed. This is taken into account by adding an additional systematic uncertainty in the signal shapes.

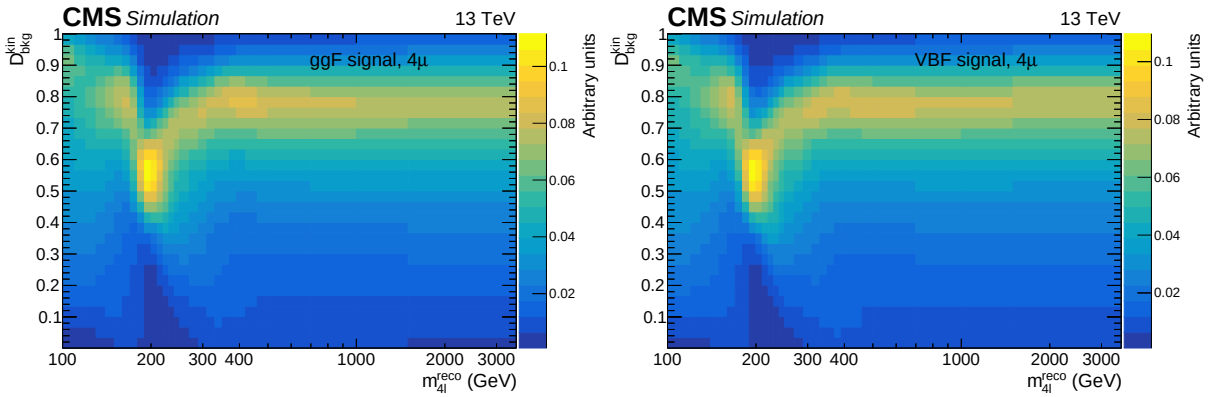


Figure 5: Expected distributions of $m^{gen}_{4\ell}$ vs. D^{kin}_{bkg} for the ggF (left) and VBF (right) production mechanisms, in the 4μ final state. The distributions are estimated from the signal simulation.

8 Background modeling

8.1 Irreducible backgrounds

The dominant background contribution comes from the $q\bar{q}ZZ$ process, with the next-largest background arising from ggZZ production. Another irreducible background is VBFZZ. Other backgrounds, including triboson production (WZZ, WWZ) and $t\bar{t}$ plus vector boson production ($t\bar{t}Z$, $t\bar{t}ZZ$, $t\bar{t}WW$), are also taken into account. All these backgrounds are estimated from simulation, with parameterized $m^{reco}_{4\ell}$ distributions to ensure consistency with the signal model, and to smooth statistical fluctuations at high mass.

The pdfs for different backgrounds are built with different methods. For $q\bar{q}ZZ$ and other backgrounds, the pdf is defined as

$$\mathcal{P}_{bkg}(m^{reco}_{4\ell}, D^{kin}_{bkg}) = \mathcal{P}(m^{reco}_{4\ell})\mathcal{P}(D^{kin}_{bkg}|m^{reco}_{4\ell}), \tag{8}$$

where the one-dimensional pdfs $\mathcal{P}(m^{reco}_{4\ell})$ are empirical functions obtained from the simulated $m^{reco}_{4\ell}$ distributions, and the conditional pdfs $\mathcal{P}(D^{kin}_{bkg}|m^{reco}_{4\ell})$ are obtained from the $m^{reco}_{4\ell}$ versus D^{kin}_{bkg} distributions in simulation.

For ggZZ and VBFZZ, the one-dimensional pdf is built using $m^{gen}_{4\ell}$ instead of $m^{reco}_{4\ell}$ because, as backgrounds that interfere with signals, their generator-level lineshapes are required to derive the interference terms introduced in Section 9. The pdf is convolved with the energy resolution function introduced in Section 7 to build the $m^{reco}_{4\ell}$ pdf. It is then multiplied by the conditional pdf $\mathcal{P}(D^{kin}_{bkg}|m^{reco}_{4\ell})$ extracted from MC simulation.

The production of a 125 GeV Higgs boson is also an irreducible background to this analysis; this process is modeled using the same approach as for the signals, by setting $m_X = 125\,\text{GeV}$ and $\Gamma_X = 4.1\,\text{MeV}$ in Eq. (5).

The expected yields of all the backgrounds described above are estimated from simulation.

8.2 Reducible backgrounds

The reducible backgrounds involve at least one selected lepton originating from the misidentification of a light jet, or from nonprompt decays of mesons or heavy-flavor jets. They are dominated by the Drell–Yan process, and also arise from other processes including $t\bar{t}$, WZ, WW, and QCD multijet events. These background processes are labelled Z + jets. The Z + jets

contribution is estimated from dedicated control regions in data, using the misidentification rate method of Refs. [24, 56]. The Z + jets yield in the signal region is evaluated by multiplying the yields extracted in the control regions by the estimated lepton misidentification rates, denoted as f_e and f_μ. These rates are defined as the fraction of leptons satisfying all the lepton selection criteria in Section 4 except the identification and isolation requirements, to that of leptons also satisfying the identification and isolation requirements. The values of f_e and f_μ are measured in another control region containing events with one Z candidate composed of two leptons satisfying all the selection criteria, plus exactly one additional lepton (e or μ) without the identification and isolation requirements. This region is denoted as $Z + \ell$. The misidentification rates are measured as functions of p_T^ℓ, separately for the barrel and endcap regions.

Two methods are used to estimate the Z + jets contribution: the opposite-sign (OS) and same-sign (SS) methods. In the OS method, the Z candidate in the $Z + \ell$ region is required to have $|m_Z - m_Z^{nom}| < 7\,GeV$ to improve purity; the control region used to estimate the event yield requires one Z candidate satisfying all the selection criteria, together with two additional OS leptons, at least one of which fails the identification and isolation requirements. In the SS method, the mass window considered in the $Z + \ell$ region is not constrained, but a dedicated approach is used to estimate the contribution of photon conversions; the control region used to estimate the event yield is defined by one Z candidate satisfying all the selections, together with two additional SS leptons, both without the identification and isolation requirements. The estimated yields from the two methods are compatible within uncertainties; the final yield estimate is taken as the average of the two estimates, weighted by their statistical uncertainties, for each final state and data-taking period. The differential distributions for the variables used in the analysis are obtained from the SS method, because the OS method introduces much larger statistical fluctuations.

The pdf for the Z + jets background is built similarly to Eq. (8), where $\mathcal{P}(m_{4\ell}^{reco})$ is the empirical function built from the Landau distribution [66], fitted to the $m_{4\ell}^{reco}$ distribution from the SS method. The conditional probability $\mathcal{P}(D_{bkg}^{kin}|m_{4\ell}^{reco})$ is obtained from the $m_{4\ell}^{reco}$ versus D_{bkg}^{kin} distribution from the SS method.

9 Interference modeling

In this analysis, the broad-width hypothesis is considered in addition to the narrow-width assumption (NWA). Therefore, the interference of the signal with other processes needs to be considered, as it can be significant when the signal width is large. The modeling of the interference follows the approach used in Ref. [9]. For the ggF (VBF) production mode, three possible interference contributions among the ggF (VBF) signal, ggF (VBF) 125 GeV Higgs boson production, and the ggZZ (VBFZZ) background are considered. The ggZZ and VBFZZ backgrounds will be referred to as nonresonant backgrounds in what follows. Interference terms are added to the signal and background models in the final statistical analysis. In particular, the interference between the 125 GeV Higgs boson production and nonresonant backgrounds is treated as a background since it is not related to signal processes. The pdf of each source of interference is built as

$$\mathcal{P}_{int}(m_{4\ell}^{reco}, D_{bkg}^{kin}) = [\mathcal{P}_{int}(m_{4\ell}^{gen}|\mathcal{P}_{sig}(m_{4\ell}^{gen}), \mathcal{P}_{bkg}(m_{4\ell}^{gen}), \text{ME phases}) \otimes \mathcal{R}(m_{4\ell}^{reco}|m_{4\ell}^{gen})]\mathcal{P}(D_{bkg}^{kin}|m_{4\ell}^{reco}). \quad (9)$$

The interference lineshape $\mathcal{P}_{\text{int}}(m_{4\ell}^{\text{gen}}|\mathcal{P}_{\text{sig}}(m_{4\ell}^{\text{gen}}), \mathcal{P}_{\text{bkg}}(m_{4\ell}^{\text{gen}}), \text{ME phases})$ contains contributions from both the amplitudes and phases of the two interfering processes. The amplitudes are extracted from the lineshapes of the signals, SM Higgs boson production, and nonresonant backgrounds. The phases of the scalar propagators (signals and 125 GeV Higgs boson) are computed from the kinematical properties, whereas the phases in other parts of the MEs are derived from the corresponding generators.

The resolution functions are the same as those for the signals introduced in Section 7, which are universal for any process with four genuine leptons.

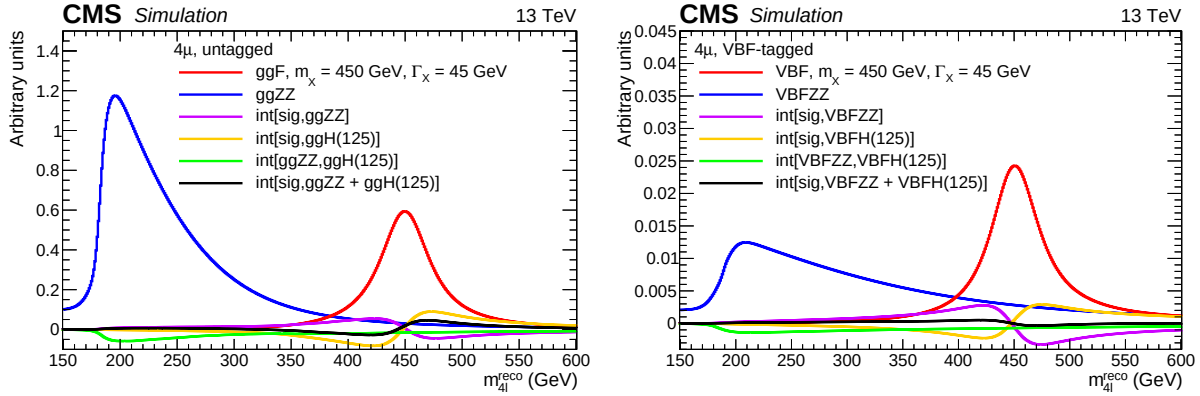


Figure 6: The left (right) plot depicts the lineshapes for the ggF (VBF) signal with $m_X = 450\,\text{GeV}$, $\Gamma_X = 45\,\text{GeV}$ as the red curve, the ggZZ (VBFZZ) background as the blue curve, and interference terms as the violet, orange, and green curves. The black curve shows the interference between the signal and all other SM processes. The notation "int[A,B]" indicates the interference between A and B. Results are shown for the 4μ final state, for the untagged category (left) and the VBF-tagged category (right).

Figure 6 shows examples of interference lineshapes, alongside the corresponding signal and nonresonant backgrounds.

The backgrounds are normalized assuming their cross sections in the SM, signals are normalized such that their cross sections are $\sigma(\text{pp} \to \text{X} \to \text{ZZ}) = 0.1\,\text{pb}$, and the interference contributions are normalized accordingly. The interference between the 125 GeV Higgs boson and the nonresonant backgrounds is mostly negative at $m_{4\ell}^{\text{gen}} > 150\,\text{GeV}$, as shown in Fig. 6. The interference between the signal and the 125 GeV Higgs boson and the interference between the signal and nonresonant backgrounds have opposite signs in the region close to the signal, and almost cancel each other out in the VBF scenario.

The conditional pdf $\mathcal{P}(D_{\text{bkg}}^{\text{kin}}|m_{4\ell}^{\text{reco}})$ for the interference terms is obtained from the $m_{4\ell}^{\text{reco}}$ versus $D_{\text{bkg}}^{\text{kin}}$ distribution extracted from MC samples reweighted using MELA variables to simulate the interference processes. Signal samples, as well as samples combining Higgs boson production, interfering backgrounds, and interference, are weighted using variables computed by MELA to estimate the interference contributions among the signal process, the 125 GeV Higgs boson, and the interfering backgrounds. The $D_{\text{bkg}}^{\text{kin}}$ distributions for interference processes are similar to those of signal processes at a given $m_{4\ell}^{\text{reco}}$.

The interference model is validated by comparing the $m_{4\ell}^{\text{reco}}$ shape from the interference model to the $m_{4\ell}^{\text{reco}}$ distribution obtained from MC simulation. Some discrepancies are observed for the interference between signals and nonresonant backgrounds, as well as between the 125 GeV Higgs boson and nonresonant backgrounds, stemming from the possible imperfect estimation

of the phases used in Eq. (9). Correction factors are computed as the ratios between the distribution from simulation and the interference model. These correction factors range from 1 to 1.3 and are applied to the interference model. Additional systematic uncertainties are estimated to cover the residual model-simulation difference, ranging from 9.5% to 11% for ggF production and 13% to 18% for VBF production.

10 Systematic uncertainties

In this analysis, more than 90% of the total uncertainty arises from statistical fluctuations in the data. However, it is still important to have a proper estimation and treatment of systematic uncertainties.

Systematic uncertainties are divided into experimental and theoretical uncertainties. Experimental uncertainties arise from imperfect knowledge of the detector and experimental measurements; theoretical uncertainties originate from the limited precision of the theoretical computations. They can affect the normalization or the shapes of each signal, background, and interference process.

10.1 Experimental uncertainties

The integrated luminosities are measured individually in the 2016, 2017, and 2018 data-taking periods [21–23]. The uncertainties range from 1% to 3%, and are partially correlated among the different years, leading to an overall 1.6% uncertainty. They affect the normalization of all processes estimated from simulation, i.e., all except Z + jets.

The lepton efficiency uncertainties arise from all the selection steps, and include trigger, reconstruction, and selection efficiencies. These uncertainties are dominated by the uncertainties in the lepton identification and isolation efficiency, and affect the yields of all the processes estimated from MC simulation. The lepton efficiency is measured with a tag-and-probe method, in both observed data and simulation. The same method as in Ref. [56] is used to extract the uncertainties. Electrons and muons are treated as uncorrelated, because the selection of these objects is different. For electrons, the uncertainty ranges from 3% to 11% in the 4e final state, and from 2% to 6% in the 2e2μ final state. For muons, the uncertainty ranges from 0.2% to 2% in the 4μ final state, and from 0.2% to 1.4% in the 2e2μ final state.

The uncertainties are computed individually for each process. For the ggF and VBF signals, the uncertainty values depend on the resonance masses. A parametrization is therefore built as a function of $m_{4\ell}^{\text{gen}}$, and used to compute the uncertainty for any signal mass.

The lepton energy scale and resolution impact the shapes of processes convolved with the energy resolution function, including signal processes, interference contributions, and interfering backgrounds. Uncertainties for electrons and muons are considered uncorrelated. The uncertainties are estimated by comparing the $Z \to \ell\ell$ invariant mass distributions in the simulation with those from the observed data. The energy scale uncertainty is 0.15% (0.03%) for electrons (muons), and it affects the final states containing electrons (muons) by shifting the μ_{res} in Eq. (6). The energy resolution uncertainty is 10% (3%) for electrons (muons), and it affects the final states containing electrons (muons) by modifying the σ_{res} in Eq. (6). The quoted values are taken from Ref. [67].

The jet energy scale and resolution do not affect the total signal or background efficiency, but affect the categorization, since the VBF tagging criteria include jet selections. These uncertainties affect all processes except Z + jets. Jet energy scale uncertainties originate from various

sources, and they are partially correlated among data-taking periods, while the uncertainty in the jet energy resolution is considered uncorrelated among all final states and data-taking periods. In general, these uncertainties amount to around 0.1% for the untagged category and 1% to 4% for the VBF-tagged category.

The jet b tagging efficiency uncertainties also affect the VBF categorization efficiency, similarly to the jet energy scale and resolution. To estimate them, the b tagging efficiencies are varied by their uncertainties, the number of jets that satisfy the b tagging requirements is recounted, and the shifted categorization is performed. These uncertainties are estimated to be smaller than 0.1%.

Simulated samples of events are corrected for the timing shift of the L1 trigger in 2016, and for mismodeling of PU distributions. The corresponding uncertainties affect the normalization of all processes, except Z + jets. These uncertainties are typically smaller than 1%, and are treated as uncorrelated between data-taking periods.

For the signal processes, uncertainties related to jets, PU, and the L1 timing shift effect are averaged over all mass points, since no mass dependence is observed.

The Z + jets estimation uncertainties take into account the statistical fluctuations in control regions. Owing to differences in the composition between the control regions where the misidentification rates are computed and where they are applied, an additional systematic uncertainty is considered. The differences are estimated using simulation, and lead to an uncertainty of around 30% on the yield of Z + jets in the SR. The uncertainty is treated as uncorrelated among final states and data-taking periods.

10.2 Theoretical uncertainties

Theoretical uncertainties are correlated across all data-taking periods.

The uncertainty in the branching fraction of $\mathrm{H} \to \mathrm{ZZ} \to 4\ell$ affects the normalization of the 125 GeV Higgs boson production processes. The uncertainty amounts to around 2% [68].

The uncertainty in the renormalization and factorization scales ($\mu_\mathrm{R}, \mu_\mathrm{F}$) is determined by simultaneously varying these two scales between 0.5 and 2 times their nominal value. This uncertainty affects all processes except the Z + jets background, and it ranges from 1% to 15% depending on the process, final state, and category. For the qqZZ background, this uncertainty affects the $m_{4\ell}^{\mathrm{reco}}$ shape in addition to the yield.

The uncertainty in the PDFs follows the PDF4LHC recommendations, taking the root-mean-square of variations with different replicas of the default NNPDF set [69]. The uncertainty in the strong coupling constant α_S is estimated by varying its value by 1 standard deviation (SD). The uncertainties range from 0.1% to 7%. For the qqZZ background, the uncertainty in the PDFs affects the $m_{4\ell}^{\mathrm{reco}}$ shape, just as for the μ_R and μ_F scales.

For the signal processes, the uncertainties in the renormalization and factorization scales, PDFs, and α_S are parameterized as a function of $m_{4\ell}^{\mathrm{gen}}$. For a given signal process, its lineshape is weighted by the parameterized function, and the uncertainty is computed as the difference in normalization between the weighted and nominal lineshapes.

The initial-state radiation (ISR) and FSR scales are used by PYTHIA [49] to model the underlying event, as well as the fragmentation and hadronization of partons. They affect all simulated processes. The uncertainties are estimated by varying the ISR and FSR scales from 4 to 0.25 times the nominal values. The uncertainty ranges from 0.4% to 10%. For the signal processes,

the values are averaged over all mass points.

An uncertainty is added to the signal and interference processes to account for potential differences in the lineshapes obtained from different generators. It ranges from 2% to 10%. Additionally, the uncertainties accounting for the interference term mismodeling introduced in Section 9 are taken into account. They range from 9.5% to 11% for ggF production, and from 13% to 18% for VBF production.

A 10% uncertainty in the determination of the K factor used for the $\mathrm{gg} \to \mathrm{ZZ}$ prediction is applied. For the $\mathrm{q\overline{q}} \to \mathrm{ZZ}$ background, the uncertainties affect the $m_{4\ell}^{\mathrm{reco}}$ shape, ranging from 0.1% at low mass to 30% at high mass.

All systematic uncertainties are treated as nuisance parameters in the fit. They are summarized in Table 1.

Table 1: Summary of the experimental and theoretical uncertainties used in this analysis. Uncertainties affecting only the normalization are marked as "norm" in the table. Those affecting observable shapes are indicated as "shape".

Source	Value	Effect	Affected processes
Experimental uncertainties			
Integrated luminosity	1.6%	norm	all except Z + jets
$\mathrm{e}(\mu)$ efficiency	2–11 (0.2–2)%	norm	all except Z + jets
$\mathrm{e}(\mu)$ energy scale	0.15 (0.03)%	shape	mass convolution
$\mathrm{e}(\mu)$ energy resolution	10 (3)%	shape	mass convolution
Jet energy scale	$\approx$1%	norm	all except Z + jets
Jet energy resolution	$\approx$1%	norm	all except Z + jets
Jet b tagging efficiency	0.1%	norm	all except Z + jets
PU and L1 timing shift	0–1%	norm	all except Z + jets
Z + jets estimation	31%	norm	Z + jets
Theoretical uncertainties			
Branching fraction of $\mathrm{H} \to \mathrm{ZZ}$	2%	norm	SM H
μ_{R}, μ_{F} scales	1–15%	qqZZ: shape others: norm	all except Z + jets
PDF	0.1–7%	qqZZ: shape others: norm	all except Z + jets
α_{S}	0.1–7%	norm	all except Z + jets
ISR, FSR scales	0.4–10%	norm	all except Z + jets
Generator modeling	2–10%	shape	signal and interference
Interference modeling	9–18%	norm	interference
qqZZ K factor	0.1–30%	shape	qqZZ
ggZZ K factor	10%	norm	ggZZ

11 Results

To build the complete statistical model, the signal strength is defined as

$$r = \frac{\sigma(\mathrm{pp} \to \mathrm{X} \to \mathrm{ZZ})}{\sigma_{\mathrm{model}}(\mathrm{pp} \to \mathrm{X} \to \mathrm{ZZ})}, \tag{10}$$

where $\sigma(\mathrm{pp} \to \mathrm{X} \to \mathrm{ZZ})$ refers to the production cross section of the resonance multiplied by the branching fraction for $\mathrm{X} \to \mathrm{ZZ}$; $\sigma_{\mathrm{model}}(\mathrm{pp} \to \mathrm{X} \to \mathrm{ZZ})$ is the reference value set in the

statistical model. The fraction of the VBF signal is defined as the VBF production cross section divided by the total production cross section:

$$f_{\mathrm{VBF}} = \frac{\sigma(\mathrm{qq} \to \mathrm{X} \to \mathrm{ZZ})}{\sigma(\mathrm{pp} \to \mathrm{X} \to \mathrm{ZZ})} = \frac{\sigma(\mathrm{qq} \to \mathrm{X} \to \mathrm{ZZ})}{\sigma(\mathrm{gg} \to \mathrm{X} \to \mathrm{ZZ}) + \sigma(\mathrm{qq} \to \mathrm{X} \to \mathrm{ZZ})}, \tag{11}$$

such that the signal strengths for ggF production and VBF production are

$$r_{\mathrm{ggF}} = r(1 - f_{\mathrm{VBF}}),\ r_{\mathrm{VBF}} = r f_{\mathrm{VBF}}. \tag{12}$$

By setting $f_{\mathrm{VBF}} = 0$ (1), the pure ggF (VBF) production mechanism hypothesis is tested.

The sum of the pdf of each process multiplied by its predicted yield is written as:

$$\mathcal{P}(\vec{x}|r,\vec{\theta}) = \sum_{\mathrm{s=ggF,VBF}} [r_{\mathrm{s}} S_{\mathrm{s}}(\vec{\theta}) \mathcal{P}_{\mathrm{s}}(\vec{x}|\vec{\theta}) + \sqrt{r_{\mathrm{s}}} I_{\mathrm{s}}(\vec{\theta}) \mathcal{P}_{\mathrm{s,int}}(\vec{x}|\vec{\theta})] + \sum_{\mathrm{b}} B_{\mathrm{b}}(\vec{\theta}) \mathcal{P}_{\mathrm{b}}(\vec{x}|\vec{\theta}). \tag{13}$$

The first sum considers the signal and interference processes, and the second sum considers all backgrounds and the 125 GeV Higgs boson-background interference. The discriminating variables are $\vec{x} = (m_{4\ell}^{\mathrm{reco}}, D_{\mathrm{bkg}}^{\mathrm{kin}})$. The expected yields for the signal, interference, and background processes are given by S_{s}, I_{s}, and B_{b}, respectively. The nuisance parameters $\vec{\theta}$ are used to take into account systematic uncertainties. Both the integrated yield and the differential distribution of each process can depend on the nuisance parameters.

Extended unbinned maximum likelihood fits are performed by fitting the background-only model to the observed data, using the COMBINE tool [70]. Figure 7 shows the comparison between the observed data and the background model with all parameters at their best fit values. The total $m_{4\ell}^{\mathrm{reco}}$ and $D_{\mathrm{bkg}}^{\mathrm{kin}}$ distributions, as well as the $m_{4\ell}^{\mathrm{reco}}$ distributions in different ranges of $D_{\mathrm{bkg}}^{\mathrm{kin}}$, are illustrated.

Upper limits at 95% confidence level (CL) on $\sigma(\mathrm{pp} \to \mathrm{X} \to \mathrm{ZZ})$ are computed, with all nuisance parameters floating and constrained based on the background-only fit. In the limit setting procedure, the $\mathrm{CL_s}$ criterion [71, 72] is used, with the profile likelihood ratio modified for upper limits as the test statistic [73]. The asymptotic approximation [74] is used to estimate the test statistic distribution. For $m_{\mathrm{X}} < 500$ GeV, the limits computed assuming the asymptotic approximation are observed to be compatible with limits set with pseudo-experiments. At high masses, as a result of the low background yields, the limits computed with the asymptotic approximation are more stringent than those computed with pseudo-experiments. However, the differences between the two approaches are found to be within 1 SD. Given the large computational resources required to perform pseudo-experiments for all signal hypotheses, the asymptotic approximation is used to compute the limits.

Figure 8 shows the results for the NWA, with Γ_{X} set to 4.1 MeV, and signal-background interference excluded. The studied value of m_{X} ranges from 130 GeV to 3 TeV. Different hypotheses for the production mechanisms are considered: pure ggF production, pure VBF production, and no assumption on the production, that is, with f_{VBF} left as a free parameter in the fit.

The exclusion limits range from 0.05–0.1 pb in the low-mass region to 0.005 pb in the high-mass region. In general, the limits are higher at 130 GeV as a result of the 125 GeV Higgs boson background, and at 200 GeV because most of the backgrounds peak in this region. The limits for the VBF production mechanism are more stringent than the limits for ggF production, as the signal-to-background ratio in the VBF tagged category is higher than in the untagged category. The results with f_{VBF} left as a free parameter are mostly similar to the results for pure ggF production, with the fitted value of f_{VBF} close to 0.

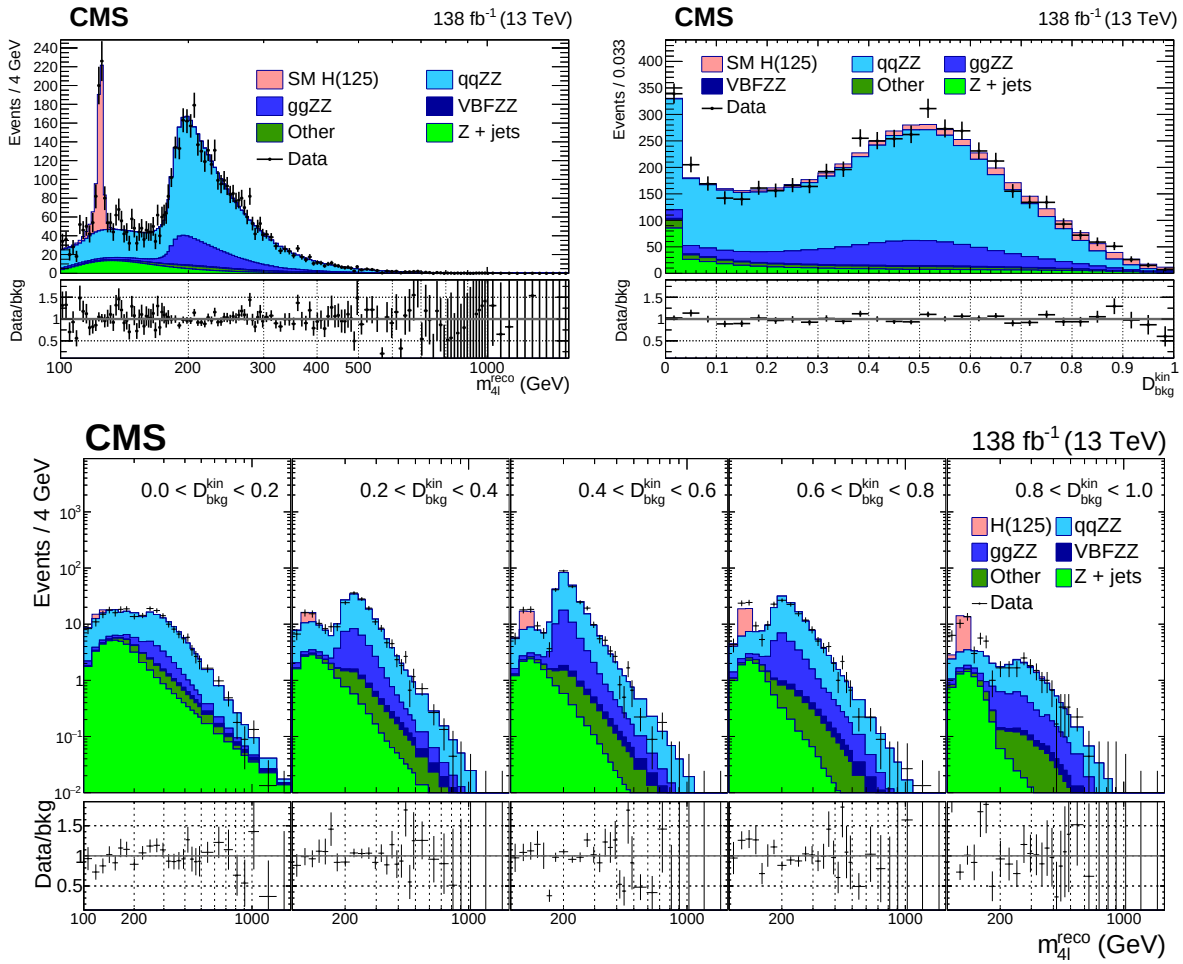


Figure 7: The $m_{4\ell}^{\text{reco}}$ and $D_{\text{bkg}}^{\text{kin}}$ distributions with the 2016–2018 data set, for backgrounds and observed data. The distributions for backgrounds are extracted from the statistical model, with all nuisance parameters at their best fit values. The upper left (right) panel shows the distribution of $m_{4\ell}^{\text{reco}}$ ($D_{\text{bkg}}^{\text{kin}}$); the lower panel shows the distribution of $m_{4\ell}^{\text{reco}}$ in bins of $D_{\text{bkg}}^{\text{kin}}$.

The local p-value [75] computed as a function of m_X is shown in Fig. 9. The local significance exceeds 2 SD at around 138, 176, 240, 280, and 360 GeV, and reaches a maximum of 3.0 SD at 137.8 GeV.

To consider the look-elsewhere effect [76], the global significance is computed by estimating the probability of finding such an excess in the 130–145 GeV mass region using 1000 toys. The global significance is found to be 1.8 SD.

In some previous studies, excesses around 600–700 GeV have been observed with global significances of 0.9–2.8 SD [11, 77, 78], which can be fitted by a resonance suggested by BSM theories [79, 80]. No such excess is found in this search.

Broad-width assumptions are also tested, with Γ_X fixed to 1, 10, or 100 GeV. The results are shown in Fig. 10. From the NWA to the 1 GeV width assumption, the limits are stronger at low masses mainly because of the off-shell production present above 200 GeV, where the signal efficiency is much higher, especially for signal masses below 200 GeV. In addition, the interference terms contribute to these stronger limits. With the decay width increasing, the limits become slightly less stringent, mainly because of the more smeared $m_{4\ell}^{\text{reco}}$ distributions.

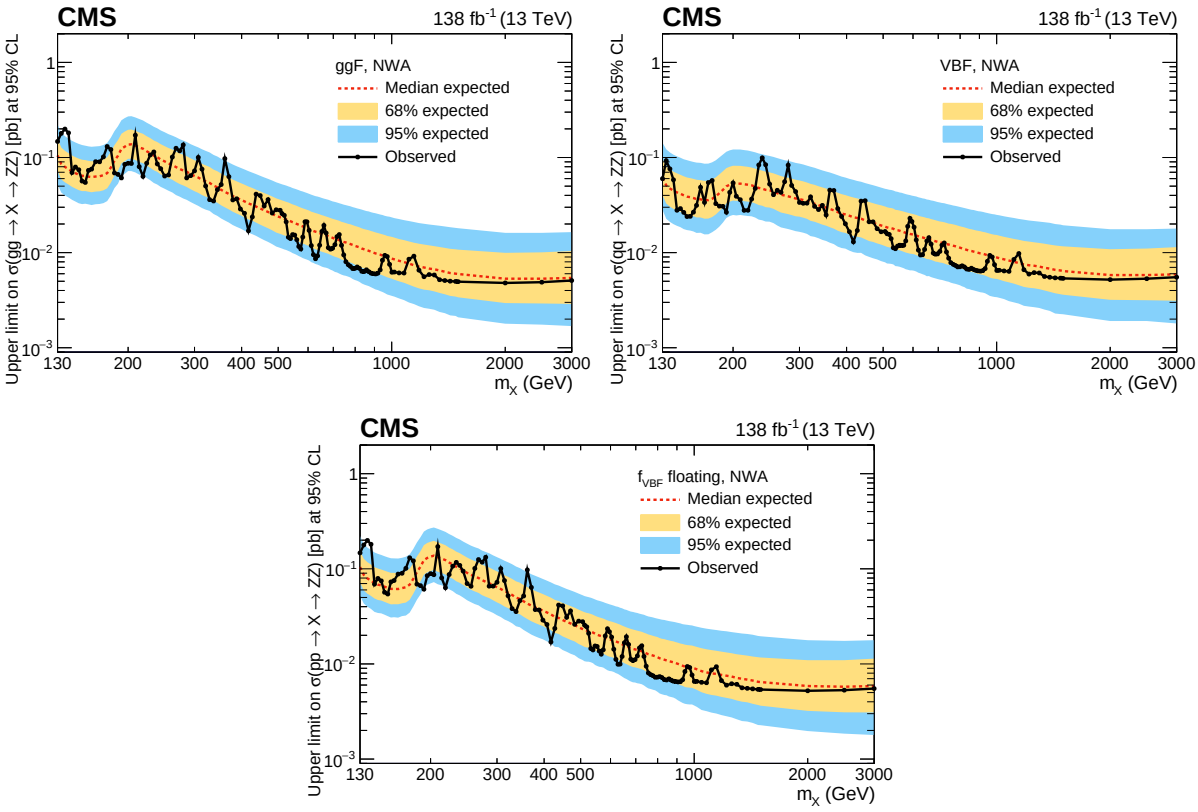


Figure 8: Observed and expected upper limits on $\sigma(\mathrm{pp} \to \mathrm{X} \to \mathrm{ZZ})$ with m_X from 130 GeV to 3 TeV in the narrow-width approximation, for the ggF (upper left) and VBF (upper right) production, and with f_VBF as a free parameter in the fit (lower).

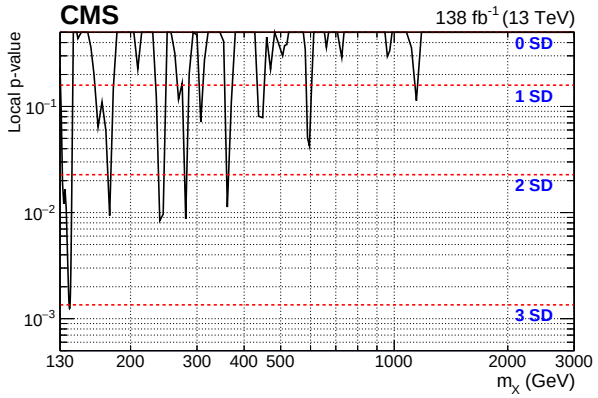


Figure 9: Local p-value as a function of m_X, with f_VBF floating.

The limits for m_X around 200 GeV, where the background contribution is the largest, become more stringent with $\Gamma_\mathrm{X} = 100$ GeV than those with $\Gamma_\mathrm{X} = 10$ GeV. The reason for this is that as the width grows, the $m_{4\ell}^\mathrm{reco}$ distribution becomes broader and more signal events fall in the region with lower background contributions.

Comparing the observed and expected results, no significant excess is observed. At $m_\mathrm{X} < 200$ GeV with $\Gamma_\mathrm{X} = 1$ and 10 GeV, as well as over the whole mass range for $\Gamma_\mathrm{X} = 100$ GeV, the observed results are systematically lower than the median expected results. The total yield of the background model is slightly larger than the number of observed events. The observed

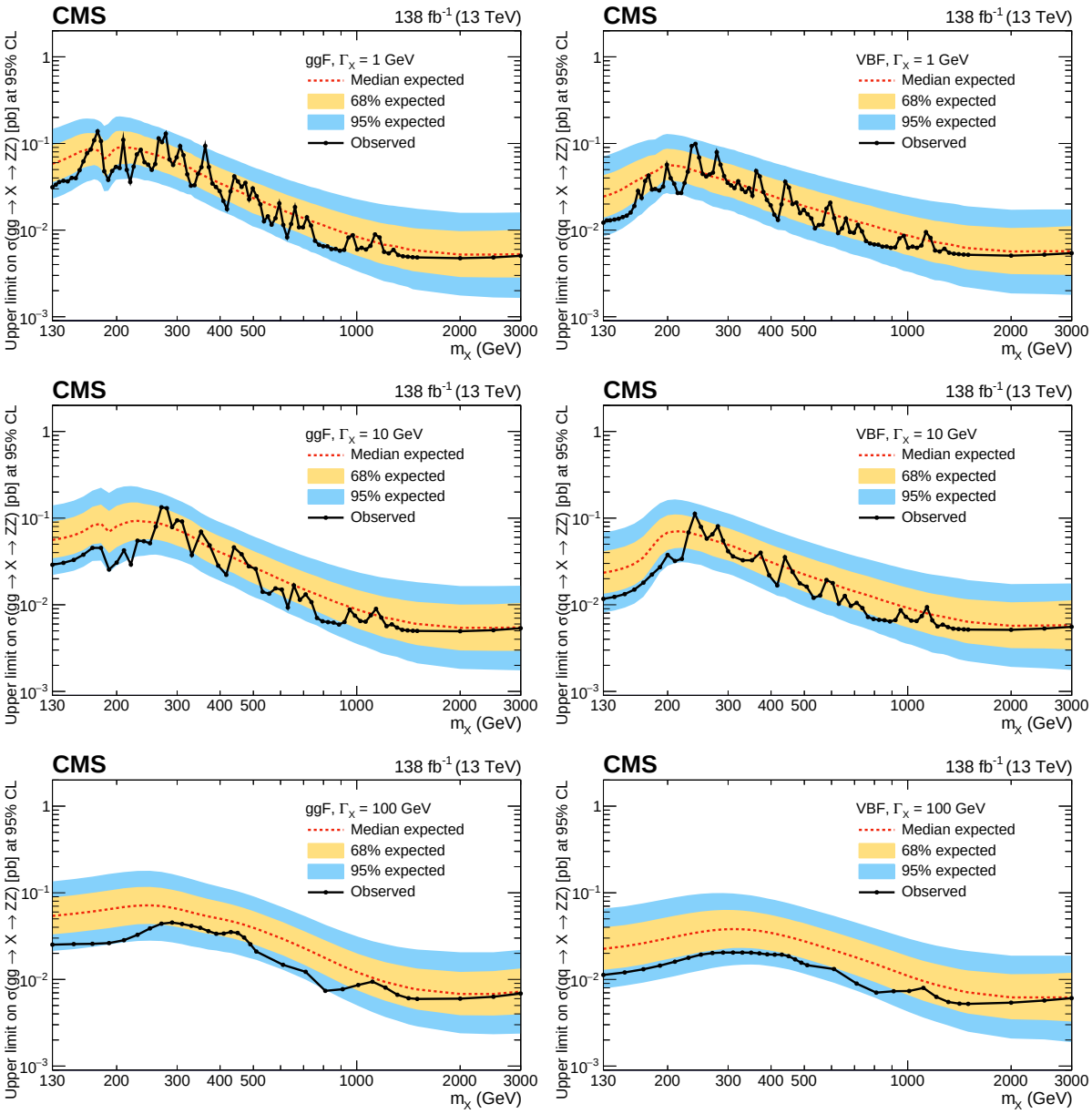


Figure 10: Observed and expected upper limits on $\sigma(\mathrm{pp} \to \mathrm{X} \to \mathrm{ZZ})$ with m_X from 130 GeV to 3 TeV and Γ_X equal to 1 (upper), 10 (middle), and 100 (lower) GeV. The left column shows the results for pure ggF production and the right column shows the results for pure VBF production.

results are, therefore, more stringent since a larger signal strength would increase the disagreement with the observed data. This is more clearly seen for the signal hypotheses that have a broad spread in their mass distribution, because the deficit of data with respect to the background expectation is correlated over a wide range through the signal lineshape. Signals at low masses ($m_\mathrm{X} < 200$ GeV) exhibit a broad spread mainly as a result of the presence of off-shell production as shown in Fig. 4. For these low-mass signals, the off-shell production contributes 50–96% for $\Gamma_\mathrm{X} = 1$ GeV, 92–98% for $\Gamma_\mathrm{X} = 10$ GeV, and greater than 99% for $\Gamma_\mathrm{X} = 100$ GeV. All signals with $\Gamma_\mathrm{X} = 100$ GeV exhibit a broad spread in the mass distribution as a result of their large width.

Results for variable m_X and Γ_X are shown in Fig. 11. Each curve corresponds to an assumption on the width, from NWA to $\Gamma_X/m_X = 0.3$. At small widths, the observed results fluctuate around the median expected limits; with the width growing, the observed results are smeared out, and excesses in the observed limits gradually disappear or move below the median expected results.

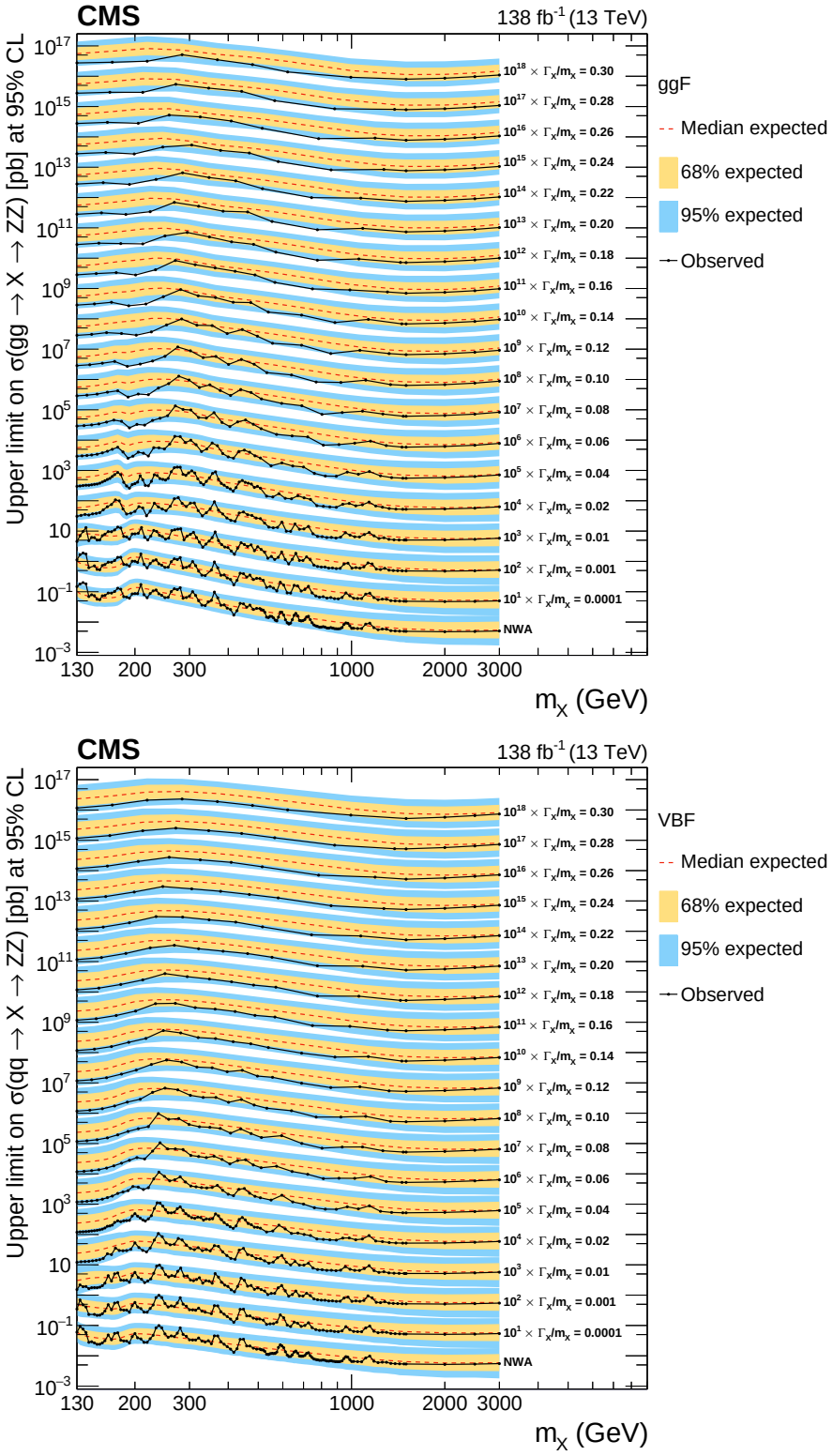


Figure 11: Observed and expected 95% CL upper limits on $\sigma(\mathrm{pp} \to X \to ZZ)$ with m_X from 130 GeV to 3 TeV and Γ_X/m_X up to 30%. The upper panel shows the results for pure ggF production, and the lower panel shows the results for pure VBF production.

12 Summary

A search for a spin-0 resonance decaying to a pair of Z bosons in the four-lepton final state, where the leptons are muons or electrons, is performed at the CMS experiment. The data set used was collected in 2016–2018 and corresponds to an integrated luminosity of 138 fb^{-1}. The searched-for resonance can be produced via gluon fusion or vector boson fusion. The mass of the sought resonance is scanned over a range from 130 GeV to 3 TeV, and different decay width assumptions are tested.

No significant excess over the standard model background expectation is observed. The largest fluctuation is seen at a mass of 137.8 GeV under the narrow-width assumption, reaching a global significance of 1.8 standard deviations. Upper limits at 95% confidence level on the production cross section multiplied by the decay branching fraction of $X \to ZZ$ are set for various masses, decay widths, and production mechanisms. The exclusion limits range from 0.05–0.1 pb in the low-mass region to 0.005 pb in the high-mass region.

Acknowledgments

We congratulate our colleagues in the CERN accelerator departments for the excellent performance of the LHC and thank the technical and administrative staffs at CERN and at other CMS institutes for their contributions to the success of the CMS effort. In addition, we gratefully acknowledge the computing centers and personnel of the Worldwide LHC Computing Grid and other centers for delivering so effectively the computing infrastructure essential to our analyses. Finally, we acknowledge the enduring support for the construction and operation of the LHC, the CMS detector, and the supporting computing infrastructure provided by the following funding agencies: SC (Armenia), BMBWF and FWF (Austria); FNRS and FWO (Belgium); CNPq, CAPES, FAPERJ, FAPERGS, and FAPESP (Brazil); MES and BNSF (Bulgaria); CERN; CAS, MoST, and NSFC (China); MINCIENCIAS (Colombia); MSES and CSF (Croatia); RIF (Cyprus); SENESCYT (Ecuador); ERC PRG and PSG, TARISTU24-TK10 and MoER TK202 (Estonia); Academy of Finland, MEC, and HIP (Finland); CEA and CNRS/IN2P3 (France); SRNSF (Georgia); BMFTR, DFG, and HGF (Germany); GSRI (Greece); MATE and NKFIH (Hungary); DAE and DST (India); IPM (Iran); SFI (Ireland); INFN (Italy); MSIT and NRF (Republic of Korea); MES (Latvia); LMTLT (Lithuania); MOE and UM (Malaysia); BUAP, CINVESTAV, CONACYT, LNS, SEP, and UASLP-FAI (Mexico); MOS (Montenegro); MBIE (New Zealand); PAEC (Pakistan); MSHE, NSC, and NAWA (Poland); FCT (Portugal); MESTD (Serbia); MICIU/AEI and PCTI (Spain); MOSTR (Sri Lanka); Swiss Funding Agencies (Switzerland); MST (Taipei); MHESI (Thailand); TUBITAK and TENMAK (Türkiye); NASU (Ukraine); STFC (United Kingdom); DOE and NSF (USA).

Individuals have received support from the Marie-Curie program and the European Research Council and Horizon 2020 Grant, contract Nos. 675440, 724704, 752730, 758316, 765710, 824093, 101115353, 101002207, 101001205, and COST Action CA16108 (European Union); the Leventis Foundation; the Alfred P. Sloan Foundation; the Alexander von Humboldt Foundation; the Science Committee, project no. 22rl-037 (Armenia); the Fonds pour la Formation à la Recherche dans l'Industrie et dans l'Agriculture (FRIA) and Fonds voor Wetenschappelijk Onderzoek contract No. 1228724N (Belgium); the Beijing Municipal Science & Technology Commission, No. Z191100007219010, the Fundamental Research Funds for the Central Universities, the Ministry of Science and Technology of China under Grant No. 2023YFA1605804, the Natural Science Foundation of China under Grant No. 12535004, and USTC Research Funds of the Double First-Class Initiative No. YD2030002017 (China); the Ministry of Edu-

cation, Youth and Sports (MEYS) of the Czech Republic; the Shota Rustaveli National Science Foundation (Georgia); the Deutsche Forschungsgemeinschaft (DFG), among others, under Germany's Excellence Strategy – EXC 2121 "Quantum Universe" – 390833306, and under project number 400140256 - GRK2497; the Hellenic Foundation for Research and Innovation (HFRI), Project Number 2288 (Greece); the Hungarian Academy of Sciences, the New National Excellence Program - ÚNKP, the NKFIH research grants K 131991, K 138136, K 143460, K 143477, K 147557, K 146913, K 146914, K 147048, TKP2021-NKTA-64, and 2025-1.1.5-NEMZ_KI-2025-00004, and MATE KKP and KKPCs Research Excellence and Flagship Research Groups grants (Hungary); the Council of Science and Industrial Research, India; ICSC – National Research Center for High Performance Computing, Big Data and Quantum Computing, FAIR – Future Artificial Intelligence Research, and CUP I53D23001070006 (Mission 4 Component 1), funded by the NextGenerationEU program, the Italian Ministry of University and Research (MUR) under Bando PRIN 2022 – CUP I53C24002390006, PRIN PRIMULA 2022RBYK7T (Italy); the Latvian Council of Science; the Ministry of Science and Higher Education, project no. 2022/WK/14, and the National Science Center, contracts Opus 2021/41/B/ST2/01369, 2021/43/B/ST2/01552, 2023/49/B/ST2/03273, and the NAWA contract BPN/PPO/2021/1/00011 (Poland); the Fundação para a Ciência e a Tecnologia (Portugal); the National Priorities Research Program by Qatar National Research Fund; MICIU/AEI/10.13039/501100011033, ERDF/EU, "European Union NextGenerationEU/PRTR", projects PID2022-142604OB-C21, PID2022-139519OB-C21, PID2023-147706NB-I00, PID2023-148896NB-I00, PID2023-146983NB-I00, PID2023-147115NB-I00, PID2023-148418NB-C41, PID2023-148418NB-C42, PID2023-148418NB-C43, PID2023-148418NB-C44, PID2024-158190NB-C22, RYC2021-033305-I, RYC2024-048719-I, CNS2023-144781, CNS2024-154769 and Plan de Ciencia, Tecnología e Innovación de Asturias, Spain; the Chulalongkorn Academic into Its 2nd Century Project Advancement Project, the National Science, Research and Innovation Fund program IND_FF_68_369_2300_097, and the Program Management Unit for Human Resources & Institutional Development, Research and Innovation, grant B39G680009 (Thailand); the Eric & Wendy Schmidt Fund for Strategic Innovation through the CERN Next Generation Triggers project under grant agreement number SIF-2023-004; the Kavli Foundation; the Nvidia Corporation; the SuperMicro Corporation; the Welch Foundation, contract C-1845; and the Weston Havens Foundation (USA).

References

[1] ATLAS Collaboration, "Observation of a new particle in the search for the standard model Higgs boson with the ATLAS detector at the LHC", *Phys. Lett. B* **716** (2012) 1, doi:10.1016/j.physletb.2012.08.020, arXiv:1207.7214.

[2] CMS Collaboration, "Observation of a new boson at a mass of 125 GeV with the CMS experiment at the LHC", *Phys. Lett. B* **716** (2012) 30, doi:10.1016/j.physletb.2012.08.021, arXiv:1207.7235.

[3] CMS Collaboration, "Observation of a new boson with mass near 125 GeV in pp collisions at $\sqrt{s} = 7$ and 8 TeV", *JHEP* **06** (2013) 81, doi:10.1007/JHEP06(2013)081, arXiv:1303.4571.

[4] G. C. Branco et al., "Theory and phenomenology of two-Higgs-doublet models", *Phys. Rept.* **516** (2012) 1, doi:10.1016/j.physrep.2012.02.002, arXiv:1106.0034.

[5] L. Randall and R. Sundrum, "Large mass hierarchy from a small extra dimension", *Phys. Rev. Lett.* **83** (1999) 3370, doi:10.1103/PhysRevLett.83.3370, arXiv:hep-ph/9905221.

[6] W. D. Goldberger and M. B. Wise, "Modulus stabilization with bulk fields", *Phys. Rev. Lett.* **83** (1999) 4922, doi:10.1103/PhysRevLett.83.4922, arXiv:hep-ph/9907447.

[7] A. Carvalho, "Gravity particles from warped extra dimensions, predictions for LHC", 2018. arXiv:1404.0102.

[8] CMS Collaboration, "Search for a Higgs boson in the mass range from 145 to 1000 GeV decaying to a pair of W or Z bosons", *JHEP* **10** (2015) 144, doi:10.1007/JHEP10(2015)144, arXiv:1504.00936.

[9] CMS Collaboration, "Search for a new scalar resonance decaying to a pair of Z bosons in proton-proton collisions at $\sqrt{s} = 13$ TeV", *JHEP* **06** (2018) 127, doi:10.1007/JHEP06(2018)127, arXiv:1804.01939.

[10] ATLAS Collaboration, "Search for an additional, heavy Higgs boson in the $h \to zz$ decay channel at $\sqrt{s} = 8$ TeV in pp collision data with the ATLAS detector", *Eur. Phys. J. C* **76** (2016) 45, doi:10.1140/epjc/s10052-015-3820-z, arXiv:1507.05930.

[11] ATLAS Collaboration, "Search for heavy resonances decaying into a pair of Z bosons in the $\ell^+\ell^-\ell'^+\ell'^-$ and $\ell^+\ell^-\nu\bar{\nu}$ final states using 139 fb^{-1} of proton–proton collisions at $\sqrt{s} = 13$ TeV with the ATLAS detector", *Eur. Phys. J. C* **81** (2021) 332, doi:10.1140/epjc/s10052-021-09013-y, arXiv:2009.14791.

[12] HEPData record for this analysis, 2026. doi:10.17182/hepdata.172455.

[13] CMS Collaboration, "The CMS experiment at the CERN LHC", *JINST* **3** (2008) S08004, doi:10.1088/1748-0221/3/08/S08004.

[14] CMS Collaboration, "Development of the CMS detector for the CERN LHC Run 3", *JINST* **19** (2024) P05064, doi:10.1088/1748-0221/19/05/P05064, arXiv:2309.05466.

[15] CMS Collaboration, "Performance of the CMS Level-1 trigger in proton-proton collisions at $\sqrt{s} = 13$ TeV", *JINST* **15** (2020) P10017, doi:10.1088/1748-0221/15/10/P10017, arXiv:2006.10165.

[16] CMS Collaboration, "The CMS trigger system", *JINST* **12** (2017) P01020, doi:10.1088/1748-0221/12/01/P01020, arXiv:1609.02366.

[17] CMS Collaboration, "Performance of the CMS high-level trigger during LHC Run 2", *JINST* **19** (2024) P11021, doi:10.1088/1748-0221/19/11/P11021, arXiv:2410.17038.

[18] CMS Collaboration, "Electron and photon reconstruction and identification with the CMS experiment at the CERN LHC", *JINST* **16** (2021) P05014, doi:10.1088/1748-0221/16/05/P05014, arXiv:2012.06888.

[19] CMS Collaboration, "Performance of the CMS muon detector and muon reconstruction with proton-proton collisions at $\sqrt{s} = 13$ TeV", *JINST* **13** (2018) P06015, doi:10.1088/1748-0221/13/06/P06015, arXiv:1804.04528.

[20] CMS Collaboration, "Description and performance of track and primary-vertex reconstruction with the CMS tracker", *JINST* **9** (2014) P10009, doi:10.1088/1748-0221/9/10/P10009, arXiv:1405.6569.

[21] CMS Collaboration, "Precision luminosity measurement in proton-proton collisions at $\sqrt{s} = 13$ TeV in 2015 and 2016 at CMS", *Eur. Phys. J. C* **81** (2021) 800, doi:10.1140/epjc/s10052-021-09538-2, arXiv:2104.01927.

[22] CMS Collaboration, "CMS luminosity measurement for the 2017 data-taking period at $\sqrt{s} = 13$ TeV", CMS Physics Analysis Summary CMS-PAS-LUM-17-004, 2018.

[23] CMS Collaboration, "CMS luminosity measurement for the 2018 data-taking period at $\sqrt{s} = 13$ TeV", CMS Physics Analysis Summary CMS-PAS-LUM-18-002, 2019.

[24] CMS Collaboration, "Measurements of production cross sections of the Higgs boson in the four-lepton final state in proton–proton collisions at $\sqrt{s} = 13$ TeV", *Eur. Phys. J. C* **81** (2021) 488, doi:10.1140/epjc/s10052-021-09200-x, arXiv:2103.04956.

[25] CMS Collaboration, "Measurement of the inclusive W and Z production cross sections in pp collisions at $\sqrt{s} = 7$ TeV with the CMS experiment", *JHEP* **10** (2011) 132, doi:10.1007/JHEP10(2011)132, arXiv:1107.4789.

[26] S. Alioli, P. Nason, C. Oleari, and E. Re, "NLO vector-boson production matched with shower in POWHEG", *JHEP* **07** (2008) 060, doi:10.1088/1126-6708/2008/07/060, arXiv:0805.4802.

[27] P. Nason, "A new method for combining NLO QCD with shower Monte Carlo algorithms", *JHEP* **11** (2004) 040, doi:10.1088/1126-6708/2004/11/040, arXiv:hep-ph/0409146.

[28] S. Frixione, P. Nason, and C. Oleari, "Matching NLO QCD computations with parton shower simulations: the POWHEG method", *JHEP* **11** (2007) 070, doi:10.1088/1126-6708/2007/11/070, arXiv:0709.2092.

[29] Y. Gao et al., "Spin determination of single-produced resonances at hadron colliders", *Phys. Rev. D* **81** (2010) 075022, doi:10.1103/PhysRevD.81.075022, arXiv:1001.3396.

[30] S. Bolognesi et al., "Spin and parity of a single-produced resonance at the LHC", *Phys. Rev. D* **86** (2012) 095031, doi:10.1103/PhysRevD.86.095031, arXiv:1208.4018.

[31] I. Anderson et al., "Constraining anomalous HVV interactions at proton and lepton colliders", *Phys. Rev. D* **89** (2014) 035007, doi:10.1103/PhysRevD.89.035007, arXiv:1309.4819.

[32] A. V. Gritsan, R. Roentsch, M. Schulze, and M. Xiao, "Constraining anomalous Higgs boson couplings to the heavy flavor fermions using matrix element techniques", *Phys. Rev. D* **94** (2016) 055023, doi:10.1103/PhysRevD.94.055023, arXiv:1606.03107.

[33] S. Goria, G. Passarino, and D. Rosco, "The Higgs-boson lineshape", *Nucl. Phys. B* **864** (2012) 530, doi:10.1016/j.nuclphysb.2012.07.006, arXiv:1112.5517.

[34] G. Passarino, C. Sturm, and S. Uccirati, "Higgs pseudo-observables, second Riemann sheet and all that", *Nucl. Phys. B* **834** (2010) 77, doi:10.1016/j.nuclphysb.2010.03.013, arXiv:1001.3360.

[35] K. Hamilton, P. Nason, E. Re, and G. Zanderighi, "NNLOPS simulation of Higgs boson production", *JHEP* **10** (2013) 222, doi:10.1007/JHEP10(2013)222, arXiv:1309.0017.

[36] M. Grazzini, S. Kallweit, and D. Rathlev, "ZZ production at the LHC: fiducial cross sections and distributions in NNLO QCD", *Phys. Lett. B* **750** (2015) 407, doi:10.1016/j.physletb.2015.09.055, arXiv:1507.06257.

[37] J. M. Campbell and R. K. Ellis, "MCFM for the Tevatron and the LHC", *Nucl. Phys. B Proc. Suppl.* **205-206** (2010) 10, doi:10.1016/j.nuclphysbps.2010.08.011, arXiv:1007.3492.

[38] J. M. Campbell, R. K. Ellis, and C. Williams, "Vector boson pair production at the LHC", *JHEP* **07** (2011) 018, doi:10.1007/JHEP07(2011)018, arXiv:1105.0020.

[39] J. M. Campbell, R. K. Ellis, and C. Williams, "Bounding the Higgs width at the LHC using full analytic results for $gg \to e^- e^+ \mu^- \mu^+$", *JHEP* **04** (2014) 060, doi:10.1007/JHEP04(2014)060, arXiv:1311.3589.

[40] M. Bonvini et al., "Signal-background interference effects for $gg \to H \to W^+W^-$ beyond leading order", *Phys. Rev. D* **88** (2013) 034032, doi:10.1103/PhysRevD.88.034032, arXiv:1304.3053.

[41] K. Melnikov and M. Dowling, "Production of two Z bosons in gluon fusion in the heavy top quark approximation", *Phys. Lett. B* **744** (2015) 43, doi:10.1016/j.physletb.2015.03.030, arXiv:1503.01274.

[42] C. S. Li, H. T. Li, D. Y. Shao, and J. Wang, "Soft gluon resummation in the signal-background interference process of $gg(\to h^*) \to ZZ$", *JHEP* **08** (2015) 65, doi:10.1007/JHEP08(2015)065, arXiv:1504.02388.

[43] S. Catani and M. Grazzini, "Next-to-next-to-leading-order subtraction formalism in hadron collisions and its application to Higgs-boson production at the Large Hadron Collider", *Phys. Rev. Lett.* **98** (2007) 222002, doi:10.1103/PhysRevLett.98.222002, arXiv:hep-ph/0703012.

[44] M. Grazzini, "NNLO predictions for the Higgs boson signal in the $H \to WW \to \ell\nu l\nu$ and $H \to ZZ \to 4\ell$ decay channels", *JHEP* **02** (2008) 043, doi:10.1088/1126-6708/2008/02/043, arXiv:0801.3232.

[45] M. Grazzini and H. Sargsyan, "Heavy-quark mass effects in Higgs boson production at the LHC", *JHEP* **09** (2013) 129, doi:10.1007/JHEP09(2013)129, arXiv:1306.4581.

[46] J. Alwall et al., "The automated computation of tree-level and next-to-leading order differential cross sections, and their matching to parton shower simulations", *JHEP* **07** (2014) 079, doi:10.1007/JHEP07(2014)079, arXiv:1405.0301.

[47] S. Frixione, P. Nason, and G. Ridolfi, "A positive-weight next-to-leading-order Monte Carlo for heavy flavour hadroproduction", *JHEP* **09** (2007) 126, doi:10.1088/1126-6708/2007/09/126, arXiv:0707.3088.

[48] A. V. Gritsan et al., "New features in the JHU generator framework: constraining Higgs boson properties from on-shell and off-shell production", *Phys. Rev. D* **102** (2020) 056022, doi:10.1103/PhysRevD.102.056022, arXiv:2002.09888.

[49] T. Sjöstrand et al., "An introduction to PYTHIA 8.2", *Comp. Phys. Commun.* **191** (2015) 159, doi:10.1016/j.cpc.2015.01.024, arXiv:1410.3012.

[50] CMS Collaboration, "Extraction and validation of a new set of CMS PYTHIA8 tunes from underlying-event measurements", *Eur. Phys. J. C* **80** (2020) 4, doi:10.1140/epjc/s10052-019-7499-4, arXiv:1903.12179.

[51] NNPDF Collaboration, "Parton distributions for the LHC Run II", *JHEP* **04** (2015) 040, doi:10.1007/JHEP04(2015)040, arXiv:1410.8849.

[52] GEANT4 Collaboration, "GEANT4—a simulation toolkit", *Nucl. Instrum. Meth. A* **506** (2003) 250, doi:10.1016/S0168-9002(03)01368-8.

[53] CMS Collaboration, "Particle-flow reconstruction and global event description with the CMS detector", *JINST* **12** (2017) P10003, doi:10.1088/1748-0221/12/10/P10003, arXiv:1706.04965.

[54] CMS Collaboration, "Technical proposal for the Phase-II upgrade of the Compact Muon Solenoid", CMS Technical Proposal CERN-LHCC-2015-010, CMS-TDR-15-02, 2015. doi:10.17181/CERN.VU8I.D59J.

[55] T. Chen and C. Guestrin, "XGBoost: A scalable tree boosting system", in *Proc. 22nd ACM SIGKDD Int. Conf. on Knowledge Discovery and Data Mining, KDD '16*, p. 785. 2016. arXiv:1603.02754. doi:10.1145/2939672.2939785.

[56] CMS Collaboration, "Measurements of inclusive and differential cross sections for the Higgs boson production and decay to four-leptons in proton-proton collisions at $\sqrt{s} = 13\,\text{TeV}$", *JHEP* **08** (2023) 40, doi:10.1007/JHEP08(2023)040, arXiv:2305.07532.

[57] CMS Collaboration, "Studies of Higgs boson production in the four-lepton final state at $\sqrt{s} = 13\,\text{TeV}$", CMS Physics Analysis Summary CMS-PAS-HIG-15-004, 2016.

[58] M. Cacciari, G. P. Salam, and G. Soyez, "The anti-k_T jet clustering algorithm", *JHEP* **04** (2008) 063, doi:10.1088/1126-6708/2008/04/063, arXiv:0802.1189.

[59] CMS Collaboration, "Jet energy scale and resolution in the CMS experiment in pp collisions at 8 TeV", *JINST* **12** (2017) P02014, doi:10.1088/1748-0221/12/02/P02014, arXiv:1607.03663.

[60] CMS Collaboration, "Pileup mitigation at CMS in 13 TeV data", *JINST* **15** (2020) P09018, doi:10.1088/1748-0221/15/09/P09018, arXiv:2003.00503.

[61] CMS Collaboration, "Identification of heavy-flavour jets with the CMS detector in pp collisions at 13 TeV", *JINST* **13** (2018) P05011, doi:10.1088/1748-0221/13/05/P05011, arXiv:1712.07158.

[62] CMS Collaboration, "Heavy flavor identification at CMS with deep neural networks", CMS Detector Performance Note CMS-DP-2017-005, 2017.

[63] CMS Collaboration, "Performance summary of AK4 jet b tagging with data from proton-proton collisions at 13 TeV with the CMS detector", CMS Detector Performance Note CMS-DP-2023-005, 2023.

[64] Particle Data Group, "Review of particle physics", *Phys. Rev. D* **110** (2024) 030001, doi:10.1103/PhysRevD.110.030001.

[65] N. Kauer and G. Passarino, "Inadequacy of zero-width approximation for a light Higgs boson signal", *JHEP* **08** (2012) 116, doi:10.1007/JHEP08(2012)116, arXiv:1206.4803.

[66] L. D. Landau, "On the energy loss of fast particles by ionisation", *J. Phys. (USSR)* **8** (1944) 417, doi:10.1016/b978-0-08-010586-4.50061-4.

[67] CMS Collaboration, "Measurement of the Higgs boson mass and width using the four-lepton final state in proton-proton collisions at $\sqrt{s} = 13\,\text{TeV}$", *Phys. Rev. D* **111** (2025) 092014, doi:10.1103/PhysRevD.111.092014, arXiv:2409.13663.

[68] LHC Higgs Cross Section Working Group, "Handbook of LHC Higgs cross sections: 4. deciphering the nature of the Higgs sector". CERN Yellow Reports: Monographs. 2017. doi:10.23731/CYRM-2017-002.

[69] J. Butterworth et al., "PDF4LHC recommendations for LHC Run II", *J. Phys. G* **43** (2016) 023001, doi:10.1088/0954-3899/43/2/023001, arXiv:1510.03865.

[70] CMS Collaboration, "The CMS statistical analysis and combination tool: COMBINE", *Comput. Softw. Big Sci.* **8** (2024) 19, doi:10.1007/s41781-024-00121-4, arXiv:2404.06614.

[71] T. Junk, "Confidence level computation for combining searches with small statistics", *Nucl. Instrum. Meth. A* **434** (1999) 435, doi:10.1016/S0168-9002(99)00498-2, arXiv:hep-ex/9902006.

[72] A. L. Read, "Presentation of search results: The CL_s technique", *J. Phys. G* **28** (2002) 2693, doi:10.1088/0954-3899/28/10/313.

[73] ATLAS and CMS Collaborations, and LHC Higgs Combination Group, "Procedure for the LHC Higgs boson search combination in Summer 2011", Technical Report CMS-NOTE-2011-005, ATL-PHYS-PUB-2011-11, 2011.

[74] G. Cowan, K. Cranmer, E. Gross, and O. Vitells, "Asymptotic formulae for likelihood-based tests of new physics", *Eur. Phys. J. C* **71** (2011) 1554, doi:10.1140/epjc/s10052-011-1554-0, arXiv:1007.1727. [Erratum: doi:10.1140/epjc/s10052-013-2501-z].

[75] L. Demortier, "P values and nuisance parameters", in *Proc. Workshop, PHYSTAT-LHC, Geneva, Switzerland, June 27-29, 2007*, p. 23. 2008. doi:10.5170/CERN-2008-001.

[76] E. Gross and O. Vitells, "Trial factors for the look elsewhere effect in high energy physics", *Eur. Phys. J. C* **70** (2010) 525, doi:10.1140/epjc/s10052-010-1470-8, arXiv:1005.1891.

[77] ATLAS Collaboration, "Search for resonances decaying into photon pairs in $139\,\text{fb}^{-1}$ of pp collisions at $\sqrt{s} = 13\,\text{TeV}$ with the ATLAS detector", *Phys. Lett. B* **822** (2021) 136651, doi:10.1016/j.physletb.2021.136651, arXiv:2102.13405.

[78] CMS Collaboration, "Search for a new resonance decaying into two spin-0 bosons in a final state with two photons and two bottom quarks in proton-proton collisions at $\sqrt{s} = 13\,\text{TeV}$", *JHEP* **05** (2024) 316, doi:10.1007/JHEP05(2024)316, arXiv:2310.01643.

[79] M. Consoli, L. Cosmai, and F. Fabbri, "Theoretical arguments and experimental signals for a second resonance of the Higgs field", *Universe* **9** (2023) 99, doi:10.3390/universe9020099.

[80] M. Consoli and G. Rupp, "Second resonance of the Higgs field: motivations, experimental signals, unitarity constraints", *Eur. Phys. J. C* **84** (2024) 951, doi:10.1140/epjc/s10052-024-13253-z, arXiv:2308.01429.

A The CMS Collaboration

Yerevan Physics Institute, Yerevan, Armenia
A. Hayrapetyan, V. Makarenko, A. Tumasyan[1]

Institut für Hochenergiephysik, Vienna, Austria
W. Adam, L. Benato, T. Bergauer, M. Dragicevic, C. Giordano, P.S. Hussain, M. Jeitler[2], N. Krammer, A. Li, D. Liko, M. Matthewman, J. Schieck[2], R. Schöfbeck[2], M. Shooshtari, M. Sonawane, W. Waltenberger, C.-E. Wulz[2]

Universiteit Antwerpen, Antwerpen, Belgium
T. Janssen, H. Kwon, D. Ocampo Henao, T. Van Laer, P. Van Mechelen

Vrije Universiteit Brussel, Brussel, Belgium
J. Bierkens, N. Breugelmans, J. D'Hondt, S. Dansana, A. De Moor, M. Delcourt, F. Heyen, Y. Hong, P. Kashko, S. Lowette, I. Makarenko, D. Müller, J. Song, S. Tavernier, M. Tytgat[3], G.P. Van Onsem, S. Van Putte, D. Vannerom

Université Libre de Bruxelles, Bruxelles, Belgium
B. Bilin, B. Clerbaux, A.K. Das, I. De Bruyn, G. De Lentdecker, H. Evard, L. Favart, P. Gianneios, A. Khalilzadeh, F.A. Khan, A. Malara, M.A. Shahzad, A. Sharma, L. Thomas, M. Vanden Bemden, C. Vander Velde, P. Vanlaer, F. Zhang

Ghent University, Ghent, Belgium
M. De Coen, D. Dobur, G. Gokbulut, D. Marckx, K. Skovpen, A.M. Tomaru, N. Van Den Bossche, J. van der Linden, J. Vandenbroeck, L. Wezenbeek

Université Catholique de Louvain, Louvain-la-Neuve, Belgium
H. Aarup Petersen, S. Bein, A. Benecke, A. Bethani, G. Bruno, A. Cappati, J. De Favereau De Jeneret, C. Delaere, F. Gameiro Casalinho, A. Giammanco, A.O. Guzel, V. Lemaitre, J. Lidrych, P. Malek, P. Mastrapasqua, S. Turkcapar

Centro Brasileiro de Pesquisas Fisicas, Rio de Janeiro, Brazil
G.A. Alves, M. Barroso Ferreira Filho, E. Coelho, C. Hensel, D. Matos Figueiredo, T. Menezes De Oliveira, C. Mora Herrera, P. Rebello Teles, M. Soeiro, E.J. Tonelli Manganote[4], A. Vilela Pereira

Universidade do Estado do Rio de Janeiro, Rio de Janeiro, Brazil
W.L. Aldá Júnior, H. Brandao Malbouisson, W. Carvalho, J. Chinellato[5], M. Costa Reis, E.M. Da Costa, G.G. Da Silveira[6], D. De Jesus Damiao, S. Fonseca De Souza, R. Gomes De Souza, S. S. Jesus, T. Laux Kuhn[6], M. Macedo, K. Mota Amarilo, L. Mundim, H. Nogima, J.P. Pinheiro, A. Santoro, A. Sznajder, M. Thiel, F. Torres Da Silva De Araujo[7]

Universidade Estadual Paulista, Universidade Federal do ABC, São Paulo, Brazil
C.A. Bernardes[6], L. Calligaris, F. Damas, T.R. Fernandez Perez Tomei, E.M. Gregores, B. Lopes Da Costa, I. Maietto Silverio, P.G. Mercadante, S.F. Novaes, B. Orzari, Sandra S. Padula, V. Scheurer

Institute for Nuclear Research and Nuclear Energy, Bulgarian Academy of Sciences, Sofia, Bulgaria
A. Aleksandrov, G. Antchev, P. Danev, R. Hadjiiska, P. Iaydjiev, M. Shopova, G. Sultanov

University of Sofia, Sofia, Bulgaria
A. Dimitrov, L. Litov, B. Pavlov, P. Petkov, A. Petrov

Instituto De Alta Investigación, Universidad de Tarapacá, Casilla 7 D, Arica, Chile
S. Keshri, D. Laroze, S. Thakur

Universidad Tecnica Federico Santa Maria, Valparaiso, Chile
W. Brooks

Beihang University, Beijing, China
T. Cheng, T. Javaid, L. Wang, L. Yuan

Department of Physics, Tsinghua University, Beijing, China
Z. Hu, Z. Liang, J. Liu, X. Wang, H. Yang

Institute of High Energy Physics, Beijing, China
G.M. Chen[8], H.S. Chen[8], M. Chen[8], Y. Chen, Q. Hou, X. Hou, F. Iemmi, C.H. Jiang, H. Liao, G. Liu, Z.-A. Liu[9], J.N. Song[9], S. Song, J. Tao, C. Wang[8], J. Wang, H. Zhang, J. Zhao

State Key Laboratory of Nuclear Physics and Technology, Peking University, Beijing, China
A. Agapitos, Y. Ban, A. Carvalho Antunes De Oliveira, S. Deng, B. Guo, Q. Guo, C. Jiang, A. Levin, C. Li, Q. Li, Y. Mao, S. Qian, S.J. Qian, X. Qin, C. Quaranta, X. Sun, D. Wang, J. Wang, M. Zhang, Y. Zhao, C. Zhou

State Key Laboratory of Nuclear Physics and Technology, Institute of Quantum Matter, South China Normal University, Guangzhou, China
S. Yang

Sun Yat-Sen University, Guangzhou, China
Z. You

University of Science and Technology of China, Hefei, China
K. Jaffel, N. Lu

Nanjing Normal University, Nanjing, China
G. Bauer[10,11], Z. Cui[11], B. Li[12], H. Wang, K. Yi[13], J. Zhang

Institute of Modern Physics and Key Laboratory of Nuclear Physics and Ion-beam Application (MOE) - Fudan University, Shanghai, China
Y. Li, Y. Zhou[14]

Zhejiang University, Hangzhou, Zhejiang, China
Z. Lin, C. Lu, M. Xiao[15]

Universidad de Los Andes, Bogota, Colombia
C. Avila, D.A. Barbosa Trujillo, A. Cabrera, C. Florez, J. Fraga, J.A. Reyes Vega

Universidad de Antioquia, Medellin, Colombia
C. Rendón, M. Rodriguez, A.A. Ruales Barbosa, J.D. Ruiz Alvarez

University of Split, Faculty of Electrical Engineering, Mechanical Engineering and Naval Architecture, Split, Croatia
N. Godinovic, D. Lelas, A. Sculac

University of Split, Faculty of Science, Split, Croatia
M. Kovac, A. Petkovic, T. Sculac

Institute Rudjer Boskovic, Zagreb, Croatia
P. Bargassa, V. Brigljevic, B.K. Chitroda, D. Ferencek, K. Jakovcic, A. Starodumov, T. Susa

University of Cyprus, Nicosia, Cyprus
A. Attikis, K. Christoforou, S. Konstantinou, C. Leonidou, L. Paizanos, F. Ptochos, P.A. Razis, H. Rykaczewski, H. Saka, A. Stepennov

Charles University, Prague, Czech Republic
M. Finger[†], M. Finger Jr.

Escuela Politecnica Nacional, Quito, Ecuador
E. Ayala

Universidad San Francisco de Quito, Quito, Ecuador
E. Carrera Jarrin

Academy of Scientific Research and Technology of the Arab Republic of Egypt, Egyptian Network of High Energy Physics, Cairo, Egypt
S. Khalil[16], E. Salama[17,18]

Center for High Energy Physics (CHEP-FU), Fayoum University, El-Fayoum, Egypt
A. Hussein, H. Mohammed

National Institute of Chemical Physics and Biophysics, Tallinn, Estonia
M. Kadastik, T. Lange, C. Nielsen, J. Pata, M. Raidal, N. Seeba, L. Tani

Department of Physics, University of Helsinki, Helsinki, Finland
E. Brücken, A. Milieva, K. Osterberg, M. Voutilainen

Helsinki Institute of Physics, Helsinki, Finland
F. Garcia, P. Inkaew, K.T.S. Kallonen, R. Kumar Verma, T. Lampén, K. Lassila-Perini, B. Lehtela, S. Lehti, T. Lindén, N.R. Mancilla Xinto, M. Myllymäki, M.m. Rantanen, S. Saariokari, N.T. Toikka, J. Tuominiemi

Lappeenranta-Lahti University of Technology, Lappeenranta, Finland
N. Bin Norjoharuddeen, H. Kirschenmann, P. Luukka, H. Petrow

IRFU, CEA, Université Paris-Saclay, Gif-sur-Yvette, France
M. Besancon, F. Couderc, M. Dejardin, D. Denegri, P. Devouge, J.L. Faure, F. Ferri, P. Gaigne, S. Ganjour, P. Gras, G. Hamel de Monchenault, M. Kumar, V. Lohezic, Y. Maidannyk, J. Malcles, F. Orlandi, L. Portales, S. Ronchi, M.Ö. Sahin, A. Savoy-Navarro[19], P. Simkina, M. Titov, M. Tornago

Laboratoire Leprince-Ringuet, CNRS/IN2P3, Ecole Polytechnique, Institut Polytechnique de Paris, Palaiseau, France
R. Amella Ranz, F. Beaudette, G. Boldrini, P. Busson, C. Charlot, M. Chiusi, T.D. Cuisset, O. Davignon, A. De Wit, T. Debnath, I.T. Ehle, S. Ghosh, A. Gilbert, R. Granier de Cassagnac, L. Kalipoliti, M. Manoni, M. Nguyen, S. Obraztsov, C. Ochando, R. Salerno, J.B. Sauvan, Y. Sirois, G. Sokmen, L. Urda Gómez, A. Zabi, A. Zghiche

Université de Strasbourg, CNRS, IPHC UMR 7178, Strasbourg, France
J.-L. Agram[20], J. Andrea, D. Bloch, J.-M. Brom, E.C. Chabert, C. Collard, G. Coulon, S. Falke, U. Goerlach, R. Haeberle, A.-C. Le Bihan, M. Meena, O. Poncet, G. Saha, P. Vaucelle

Centre de Calcul de l'Institut National de Physique Nucleaire et de Physique des Particules, CNRS/IN2P3, Villeurbanne, France
A. Di Florio

Institut de Physique des 2 Infinis de Lyon (IP2I), Villeurbanne, France
D. Amram, S. Beauceron, B. Blancon, G. Boudoul, N. Chanon, D. Contardo, P. Depasse, H. El Mamouni, J. Fay, S. Gascon, M. Gouzevitch, C. Greenberg, G. Grenier, B. Ille, E. Jourd'Huy, M. Lethuillier, B. Massoteau, L. Mirabito, A. Purohit, M. Vander Donckt, J. Xiao

Georgian Technical University, Tbilisi, Georgia
A. Khvedelidze[21], I. Lomidze, Z. Tsamalaidze[21]

RWTH Aachen University, I. Physikalisches Institut, Aachen, Germany
V. Botta, S. Consuegra Rodríguez, L. Feld, K. Klein, M. Lipinski, P. Nattland, V. Oppenländer, A. Pauls, D. Pérez Adán, N. Röwert

RWTH Aachen University, III. Physikalisches Institut A, Aachen, Germany
C. Daumann, S. Diekmann, N. Eich, D. Eliseev, F. Engelke, J. Erdmann, M. Erdmann, B. Fischer, T. Hebbeker, K. Hoepfner, F. Ivone, A. Jung, N. Kumar, M.y. Lee, F. Mausolf, M. Merschmeyer, A. Meyer, A. Pozdnyakov, W. Redjeb, H. Reithler, U. Sarkar, V. Sarkisovi, A. Schmidt, C. Seth, A. Sharma, J.L. Spah, V. Vaulin, S. Zaleski

RWTH Aachen University, III. Physikalisches Institut B, Aachen, Germany
M.R. Beckers, C. Dziwok, G. Flügge, N. Hoeflich, T. Kress, A. Nowack, O. Pooth, A. Stahl, A. Zotz

Deutsches Elektronen-Synchrotron, Hamburg, Germany
A. Abel, M. Aldaya Martin, J. Alimena, S. Amoroso, Y. An, I. Andreev, J. Bach, S. Baxter, M. Bayatmakou, H. Becerril Gonzalez, O. Behnke, A. Belvedere, F. Blekman[22], K. Borras[23], A. Campbell, S. Chatterjee, L.X. Coll Saravia, G. Eckerlin, D. Eckstein, E. Gallo[22], A. Geiser, M. Guthoff, A. Hinzmann, L. Jeppe, M. Kasemann, C. Kleinwort, R. Kogler, M. Komm, D. Krücker, W. Lange, D. Leyva Pernia, K.-Y. Lin, K. Lipka[24], W. Lohmann[25], J. Malvaso, R. Mankel, I.-A. Melzer-Pellmann, M. Mendizabal Morentin, A.B. Meyer, G. Milella, K. Moral Figueroa, A. Mussgiller, L.P. Nair, J. Niedziela, A. Nürnberg, J. Park, E. Ranken, A. Raspereza, D. Rastorguev, L. Rygaard, M. Scham[26,23], S. Schnake[23], P. Schütze, C. Schwanenberger[22], D. Schwarz, D. Selivanova, K. Sharko, M. Shchedrolosiev, D. Stafford, M. Torkian, A. Ventura Barroso, R. Walsh, D. Wang, Q. Wang, K. Wichmann, L. Wiens[23], C. Wissing, Y. Yang, S. Zakharov, A. Zimermmane Castro Santos

University of Hamburg, Hamburg, Germany
A.R. Alves Andrade, M. Antonello, S. Bollweg, M. Bonanomi, L. Ebeling, K. El Morabit, Y. Fischer, M. Frahm, E. Garutti, A. Grohsjean, A.A. Guvenli, J. Haller, D. Hundhausen, G. Kasieczka, P. Keicher, R. Klanner, W. Korcari, T. Kramer, C.c. Kuo, F. Labe, J. Lange, A. Lobanov, J. Matthiesen, L. Moureaux, K. Nikolopoulos, A. Paasch, K.J. Pena Rodriguez, N. Prouvost, B. Raciti, M. Rieger, D. Savoiu, P. Schleper, M. Schröder, J. Schwandt, M. Sommerhalder, H. Stadie, G. Steinbrück, R. Ward, B. Wiederspan, M. Wolf, C. Yede

Karlsruher Institut fuer Technologie, Karlsruhe, Germany

S. Brommer, A. Brusamolino, E. Butz, Y.M. Chen, T. Chwalek, A. Dierlamm, G.G. Dincer, D. Druzhkin, U. Elicabuk, N. Faltermann, M. Giffels, A. Gottmann, F. Hartmann[27], M. Horzela, F. Hummer, U. Husemann, J. Kieseler, M. Klute, J. Knolle, R. Kunnilan Muhammed Rafeek, O. Lavoryk, J.M. Lawhorn, A. Lintuluoto, S. Maier, A.A. Monsch, M. Mormile, Th. Müller, E. Pfeffer, M. Presilla, G. Quast, K. Rabbertz, B. Regnery, R. Schmieder, N. Shadskiy, I. Shvetsov, H.J. Simonis, L. Sowa, L. Stockmeier, K. Tauqeer, M. Toms, B. Topko, N. Trevisani, C. Verstege, T. Voigtländer, R.F. Von Cube, J. Von Den Driesch, M. Wassmer, C. Winter, R. Wolf, W.D. Zeuner, X. Zuo

Institute of Nuclear and Particle Physics (INPP), NCSR Demokritos, Aghia Paraskevi, Greece
G. Anagnostou, G. Daskalakis, A. Kyriakis

National and Kapodistrian University of Athens, Athens, Greece
G. Melachroinos, Z. Painesis, I. Paraskevas, N. Saoulidou, K. Theofilatos, E. Tziaferi, E. Tzovara, K. Vellidis, I. Zisopoulos

National Technical University of Athens, Athens, Greece
T. Chatzistavrou, G. Karapostoli, K. Kousouris, E. Siamarkou, G. Tsipolitis

University of Ioánnina, Ioánnina, Greece
I. Bestintzanos, I. Evangelou, C. Foudas, P. Katsoulis, P. Kokkas, P.G. Kosmoglou Kioseoglou, N. Manthos, I. Papadopoulos, J. Strologas

HUN-REN Wigner Research Centre for Physics, Budapest, Hungary
C. Hajdu, D. Horvath[28,29], K. Márton, A.J. Rádl[30], F. Sikler, V. Veszpremi

MTA-ELTE Lendület CMS Particle and Nuclear Physics Group, Eötvös Loránd University, Budapest, Hungary
M. Csanád, K. Farkas, A. Fehérkuti[31], M.M.A. Gadallah[32], Á. Kadlecsik, M. León Coello, G. Pásztor, G.I. Veres

Faculty of Informatics, University of Debrecen, Debrecen, Hungary
B. Ujvari, G. Zilizi

HUN-REN ATOMKI - Institute of Nuclear Research, Debrecen, Hungary
G. Bencze, S. Czellar, J. Molnar, Z. Szillasi

Karoly Robert Campus, MATE Institute of Technology, Gyongyos, Hungary
T. Csorgo[31], F. Nemes[31], T. Novak, I. Szanyi[33]

IIT Bhubaneswar, Bhubaneswar, India
S. Bahinipati, S. Nayak, R. Raturi

Panjab University, Chandigarh, India
S. Bansal, S.B. Beri, V. Bhatnagar, S. Chauhan, N. Dhingra[34], A. Kaur, H. Kaur, M. Kaur, S. Kumar, T. Sheokand, J.B. Singh, A. Singla

University of Delhi, Delhi, India
A. Bhardwaj, A. Chhetri, B.C. Choudhary, A. Kumar, A. Kumar, M. Naimuddin, S. Phor, K. Ranjan, M.K. Saini

Indian Institute of Technology Mandi (IIT-Mandi), Himachal Pradesh, India
P. Palni

University of Hyderabad, Hyderabad, India
S. Acharya[35], B. Gomber

Indian Institute of Technology Kanpur, Kanpur, India
S. Mukherjee

Saha Institute of Nuclear Physics, HBNI, Kolkata, India
S. Bhattacharya, S. Das Gupta, S. Dutta, S. Dutta, S. Sarkar

Indian Institute of Technology Madras, Madras, India
M.M. Ameen, P.K. Behera, S. Chatterjee, G. Dash, A. Dattamunsi, P. Jana, P. Kalbhor, S. Kamble, J.R. Komaragiri[36], T. Mishra, P.R. Pujahari, A.K. Sikdar, R.K. Singh, P. Verma, S. Verma, A. Vijay

IISER Mohali, India, Mohali, India
B.K. Sirasva

Tata Institute of Fundamental Research-A, Mumbai, India
L. Bhatt, S. Dugad, G.B. Mohanty, M. Shelake, P. Suryadevara

Tata Institute of Fundamental Research-B, Mumbai, India
A. Bala, S. Banerjee, S. Barman[37], R.M. Chatterjee, M. Guchait, Sh. Jain, A. Jaiswal, S. Kumar, M. Maity[37], G. Majumder, K. Mazumdar, S. Parolia, R. Saxena, A. Thachayath

National Institute of Science Education and Research, Odisha, India
D. Maity[38], P. Mal, K. Naskar[38], A. Nayak[38], K. Pal, P. Sadangi, S.K. Swain, S. Varghese[38], D. Vats[38]

Indian Institute of Science Education and Research (IISER), Pune, India
S. Dube, P. Hazarika, B. Kansal, A. Laha, R. Sharma, S. Sharma, K.Y. Vaish

Indian Institute of Technology Hyderabad, Telangana, India
S. Ghosh

Isfahan University of Technology, Isfahan, Iran
H. Bakhshiansohi[39], A. Jafari[40], V. Sedighzadeh Dalavi, M. Zeinali[41]

Institute for Research in Fundamental Sciences (IPM), Tehran, Iran
S. Bashiri, S. Chenarani[42], S.M. Etesami, Y. Hosseini, M. Khakzad, E. Khazaie, M. Mohammadi Najafabadi, S. Tizchang[43]

University College Dublin, Dublin, Ireland
M. Felcini, M. Grunewald

INFN Sezione di Bari[a], Università di Bari[b], Politecnico di Bari[c], Bari, Italy
M. Abbrescia[a,b], M. Barbieri[a,b], M. Buonsante[a,b], A. Colaleo[a,b], D. Creanza[a,c], N. De Filippis[a,c], M. De Palma[a,b], W. Elmetenawee[a,b,44], N. Ferrara[a,c], L. Fiore[a], L. Generoso[a,b], L. Longo[a], M. Louka[a,b], G. Maggi[a,c], M. Maggi[a], I. Margjeka[a], V. Mastrapasqua[a,b], S. My[a,b], F. Nenna[a,b], S. Nuzzo[a,b], A. Pellecchia[a,b], A. Pompili[a,b], G. Pugliese[a,c], R. Radogna[a,b], D. Ramos[a], A. Ranieri[a], L. Silvestris[a], F.M. Simone[a,c], Ü. Sözbilir[a], A. Stamerra[a,b], D. Troiano[a,b], R. Venditti[a,b], P. Verwilligen[a], A. Zaza[a,b]

INFN Sezione di Bologna[a], Università di Bologna[b], Bologna, Italy
G. Abbiendi[a], C. Battilana[a,b], D. Bonacorsi[a,b], P. Capiluppi[a,b], F.R. Cavallo[a],

G.M. Dallavalle[a], T. Diotalevi[a,b], F. Fabbri[a], A. Fanfani[a,b], D. Fasanella[a], P. Giacomelli[a], C. Grandi[a], L. Guiducci[a,b], S. Lo Meo[a,45], M. Lorusso[a,b], L. Lunerti[a], S. Marcellini[a], G. Masetti[a], F.L. Navarria[a,b], G. Paggi[a,b], A. Perrotta[a], A.M. Rossi[a,b], S. Rossi Tisbeni[a,b], T. Rovelli[a,b], G.P. Siroli[a,b]

INFN Sezione di Catania[a], Università di Catania[b], Catania, Italy
S. Costa[a,b,46], A. Di Mattia[a], A. Lapertosa[a], R. Potenza[a,b], A. Tricomi[a,b,46]

INFN Sezione di Firenze[a], Università di Firenze[b], Firenze, Italy
J. Altork[a,b], P. Assiouras[a], G. Barbagli[a], G. Bardelli[a], M. Bartolini[a,b], A. Calandri[a,b], B. Camaiani[a,b], A. Cassese[a], R. Ceccarelli[a], V. Ciulli[a,b], C. Civinini[a], R. D'Alessandro[a,b], L. Damenti[a,b], E. Focardi[a,b], T. Kello[a], G. Latino[a,b], P. Lenzi[a,b], M. Lizzo[a], M. Meschini[a], S. Paoletti[a], A. Papanastassiou[a,b], G. Sguazzoni[a], L. Viliani[a]

INFN Laboratori Nazionali di Frascati, Frascati, Italy
L. Benussi, S. Colafranceschi[47], S. Meola[48], D. Piccolo

INFN Sezione di Genova[a], Università di Genova[b], Genova, Italy
M. Alves Gallo Pereira[a], F. Ferro[a], E. Robutti[a], S. Tosi[a,b]

INFN Sezione di Milano-Bicocca[a], Università di Milano-Bicocca[b], Milano, Italy
A. Benaglia[a], F. Brivio[a], V. Camagni[a,b], F. Cetorelli[a,b], F. De Guio[a,b], M.E. Dinardo[a,b], P. Dini[a], S. Gennai[a], R. Gerosa[a,b], A. Ghezzi[a,b], P. Govoni[a,b], L. Guzzi[a], M.R. Kim[a], G. Lavizzari[a,b], M.T. Lucchini[a,b], M. Malberti[a], S. Malvezzi[a], A. Massironi[a], D. Menasce[a], L. Moroni[a], M. Paganoni[a,b], S. Palluotto[a,b], D. Pedrini[a], A. Perego[a,b], G. Pizzati[a,b], T. Tabarelli de Fatis[a,b]

INFN Sezione di Napoli[a], Università di Napoli 'Federico II'[b], Napoli, Italy; Università della Basilicata[c], Potenza, Italy; Scuola Superiore Meridionale (SSM)[d], Napoli, Italy
S. Buontempo[a], C. Di Fraia[a,b], F. Fabozzi[a,c], L. Favilla[a,d], A.O.M. Iorio[a,b], L. Lista[a,b,49], P. Paolucci[a,27], B. Rossi[a]

INFN Sezione di Padova[a], Università di Padova[b], Padova, Italy; Universita degli Studi di Cagliari[c], Cagliari, Italy
P. Azzi[a], N. Bacchetta[a,50], D. Bisello[a,b], L. Borella[a], P. Bortignon[a,c], G. Bortolato[a,b], A.C.M. Bulla[a,c], R. Carlin[a,b], T. Dorigo[a,51], F. Gasparini[a,b], S. Giorgetti[a], F. Gonella[a], E. Lusiani[a], M. Margoni[a,b], A.T. Meneguzzo[a,b], J. Pazzini[a,b], F. Primavera[a,b], P. Ronchese[a,b], R. Rossin[a,b], F. Simonetto[a,b], M. Tosi[a,b], A. Triossi[a,b], S. Ventura[a], M. Zanetti[a,b], P. Zotto[a,b], A. Zucchetta[a,b], G. Zumerle[a,b]

INFN Sezione di Pavia[a], Università di Pavia[b], Pavia, Italy
A. Braghieri[a], S. Calzaferri[a,b], P. Montagna[a,b], M. Pelliccioni[a,b], V. Re[a], C. Riccardi[a,b], P. Salvini[a], I. Vai[a,b], P. Vitulo[a,b]

INFN Sezione di Perugia[a], Università di Perugia[b], Perugia, Italy
S. Ajmal[a,b], M.E. Ascioti[a,b], G.M. Bilei[†a], C. Carrivale[a,b], D. Ciangottini[a,b], L. Della Penna[a,b], L. Fanò[a,b], V. Mariani[a,b], M. Menichelli[a], F. Moscatelli[a,52], A. Rossi[a,b], A. Santocchia[a,b], D. Spiga[a], T. Tedeschi[a,b]

INFN Sezione di Pisa[a], Università di Pisa[b], Scuola Normale Superiore di Pisa[c], Pisa, Italy; Università di Siena[d], Siena, Italy
C. Aimè[a,b], C.A. Alexe[a,c], P. Asenov[a,b], P. Azzurri[a], G. Bagliesi[a], L. Bianchini[a,b],

T. Boccali[a], E. Bossini[a], D. Bruschini[a,c], R. Castaldi[a], F. Cattafesta[a,c], M.A. Ciocci[a,d], M. Cipriani[a,b], R. Dell'Orso[a], S. Donato[a,b], R. Forti[a,b], A. Giassi[a], F. Ligabue[a,c], A.C. Marini[a,b], A. Messineo[a,b], S. Mishra[a], V.K. Muraleedharan Nair Bindhu[a,b], S. Nandan[a], F. Palla[a], M. Riggirello[a,c], A. Rizzi[a,b], G. Rolandi[a,c], S. Roy Chowdhury[a,53], T. Sarkar[a], A. Scribano[a], P. Solanki[a,b], P. Spagnolo[a], F. Tenchini[a,b], R. Tenchini[a], G. Tonelli[a,b], N. Turini[a,d], F. Vaselli[a,c], A. Venturi[a], P.G. Verdini[a]

INFN Sezione di Roma[a], Sapienza Università di Roma[b], Roma, Italy
P. Akrap[a,b], C. Basile[a,b], S.C. Behera[a], F. Cavallari[a], L. Cunqueiro Mendez[a,b], F. De Riggi[a,b], D. Del Re[a,b], E. Di Marco[a], M. Diemoz[a], F. Errico[a], L. Frosina[a,b], R. Gargiulo[a,b], B. Harikrishnan[a,b], F. Lombardi[a,b], E. Longo[a,b], L. Martikainen[a,b], J. Mijuskovic[a,b], G. Organtini[a,b], N. Palmeri[a,b], R. Paramatti[a,b], S. Rahatlou[a,b], C. Rovelli[a], F. Santanastasio[a,b], L. Soffi[a], V. Vladimirov[a,b]

INFN Sezione di Torino[a], Università di Torino[b], Torino, Italy; Università del Piemonte Orientale[c], Novara, Italy
N. Amapane[a,b], R. Arcidiacono[a,c], S. Argiro[a,b], M. Arneodo[†a,c], N. Bartosik[a,c], R. Bellan[a,b], A. Bellora[a,b], C. Biino[a], C. Borca[a,b], N. Cartiglia[a], M. Costa[a,b], R. Covarelli[a,b], N. Demaria[a], L. Finco[a], M. Grippo[a,b], B. Kiani[a,b], L. Lanteri[a,b], F. Legger[a], F. Luongo[a,b], C. Mariotti[a], S. Maselli[a], A. Mecca[a,b], L. Menzio[a,b], P. Meridiani[a], E. Migliore[a,b], M. Monteno[a], M.M. Obertino[a,b], G. Ortona[a], L. Pacher[a,b], N. Pastrone[a], M. Ruspa[a,c], F. Siviero[a,b], V. Sola[a,b], A. Solano[a,b], A. Staiano[a], C. Tarricone[a,b], D. Trocino[a], G. Umoret[a,b], E. Vlasov[a,b], R. White[a,b]

INFN Sezione di Trieste[a], Università di Trieste[b], Trieste, Italy
J. Babbar[a,b,53], S. Belforte[a], V. Candelise[a,b], M. Casarsa[a], F. Cossutti[a], K. De Leo[a], G. Della Ricca[a,b], R. Delli Gatti[a,b]

Kyungpook National University, Daegu, Korea
S. Dogra, J. Hong, J. Kim, T. Kim, D. Lee, H. Lee, J. Lee, S.W. Lee, C.S. Moon, Y.D. Oh, S. Sekmen, B. Tae, Y.C. Yang

Department of Mathematics and Physics - GWNU, Gangneung, Korea
M.S. Kim

Chonnam National University, Institute for Universe and Elementary Particles, Kwangju, Korea
G. Bak, P. Gwak, H. Kim, D.H. Moon, J. Seo

Hanyang University, Seoul, Korea
E. Asilar, F. Carnevali, J. Choi[54], T.J. Kim, Y. Ryou

Korea University, Seoul, Korea
S. Ha, S. Han, B. Hong, J. Kim, K. Lee, K.S. Lee, S. Lee, J. Yoo

Kyung Hee University, Department of Physics, Seoul, Korea
J. Goh, J. Shin, S. Yang

Sejong University, Seoul, Korea
Y. Kang, H. S. Kim, Y. Kim, B. Ko, S. Lee

Seoul National University, Seoul, Korea
J. Almond, J.H. Bhyun, J. Choi, J. Choi, W. Jun, H. Kim, J. Kim, T. Kim, Y. Kim, Y.W. Kim, S. Ko, H. Lee, J. Lee, J. Lee, B.H. Oh, J. Shin, U.K. Yang, I. Yoon

University of Seoul, Seoul, Korea
W. Jang, D.Y. Kang, D. Kim, S. Kim, J.S.H. Lee, Y. Lee, I.C. Park, Y. Roh, I.J. Watson

Yonsei University, Department of Physics, Seoul, Korea
G. Cho, K. Hwang, B. Kim, S. Kim, K. Lee, H.D. Yoo

Sungkyunkwan University, Suwon, Korea
Y. Lee, I. Yu

College of Engineering and Technology, American University of the Middle East (AUM), Dasman, Kuwait
T. Beyrouthy, Y. Gharbia

Kuwait University - College of Science - Department of Physics, Safat, Kuwait
F. Alazemi

Riga Technical University, Riga, Latvia
K. Dreimanis, O.M. Eberlins, A. Gaile, C. Munoz Diaz, D. Osite, G. Pikurs, R. Plese, A. Potrebko, M. Seidel, D. Sidiropoulos Kontos

University of Latvia (LU), Riga, Latvia
N.R. Strautnieks

Vilnius University, Vilnius, Lithuania
M. Ambrozas, A. Juodagalvis, S. Nargelas, A. Rinkevicius, G. Tamulaitis

National Centre for Particle Physics, Universiti Malaya, Kuala Lumpur, Malaysia
I. Yusuff[55], Z. Zolkapli

Universidad de Sonora (UNISON), Hermosillo, Mexico
J.F. Benitez, A. Castaneda Hernandez, A. Cota Rodriguez, L.E. Cuevas Picos, H.A. Encinas Acosta, L.G. Gallegos Maríñez, J.A. Murillo Quijada, L. Valencia Palomo

Centro de Investigacion y de Estudios Avanzados del IPN, Mexico City, Mexico
G. Ayala, H. Castilla-Valdez, H. Crotte Ledesma, R. Lopez-Fernandez, J. Mejia Guisao, R. Reyes-Almanza, A. Sánchez Hernández

Universidad Iberoamericana, Mexico City, Mexico
C. Oropeza Barrera, D.L. Ramirez Guadarrama, M. Ramírez García

Benemerita Universidad Autonoma de Puebla, Puebla, Mexico
I. Bautista, F.E. Neri Huerta, I. Pedraza, H.A. Salazar Ibarguen, C. Uribe Estrada

University of Montenegro, Podgorica, Montenegro
I. Bubanja, N. Raicevic

University of Canterbury, Christchurch, New Zealand
P.H. Butler

National Centre for Physics, Quaid-I-Azam University, Islamabad, Pakistan
A. Ahmad, M.I. Asghar, A. Awais, M.I.M. Awan, W.A. Khan

AGH University of Krakow, Krakow, Poland
V. Avati, L. Forthomme, L. Grzanka, M. Malawski, K. Piotrzkowski

National Centre for Nuclear Research, Swierk, Poland
M. Bluj, M. Górski, M. Kazana, M. Szleper, P. Zalewski

Institute of Experimental Physics, Faculty of Physics, University of Warsaw, Warsaw, Poland
K. Bunkowski, K. Doroba, A. Kalinowski, M. Konecki, J. Krolikowski, A. Muhammad

Warsaw University of Technology, Warsaw, Poland
P. Fokow, K. Pozniak, W. Zabolotny

Laboratório de Instrumentação e Física Experimental de Partículas, Lisboa, Portugal
M. Araujo, D. Bastos, C. Beirão Da Cruz E Silva, A. Boletti, M. Bozzo, T. Camporesi, G. Da Molin, M. Gallinaro, J. Hollar, N. Leonardo, G.B. Marozzo, A. Petrilli, M. Pisano, J. Seixas, J. Varela, J.W. Wulff

Faculty of Physics, University of Belgrade, Belgrade, Serbia
P. Adzic, L. Markovic, P. Milenovic, V. Milosevic

VINCA Institute of Nuclear Sciences, University of Belgrade, Belgrade, Serbia
D. Devetak, M. Dordevic, J. Milosevic, L. Nadderd, V. Rekovic, M. Stojanovic

Centro de Investigaciones Energéticas Medioambientales y Tecnológicas (CIEMAT), Madrid, Spain
M. Alcalde Martinez, J. Alcaraz Maestre, Cristina F. Bedoya, J.A. Brochero Cifuentes, Oliver M. Carretero, M. Cepeda, M. Cerrada, N. Colino, B. De La Cruz, A. Delgado Peris, A. Escalante Del Valle, D. Fernández Del Val, J.P. Fernández Ramos, J. Flix, M.C. Fouz, M. Gonzalez Hernandez, O. Gonzalez Lopez, S. Goy Lopez, J.M. Hernandez, M.I. Josa, J. Llorente Merino, C. Martin Perez, E. Martin Viscasillas, D. Moran, C. M. Morcillo Perez, Á. Navarro Tobar, R. Paz Herrera, A. Pérez-Calero Yzquierdo, J. Puerta Pelayo, I. Redondo, J. Vazquez Escobar

Universidad Autónoma de Madrid, Madrid, Spain
J.F. de Trocóniz

Universidad de Oviedo, Instituto Universitario de Ciencias y Tecnologías Espaciales de Asturias (ICTEA), Oviedo, Spain
B. Alvarez Gonzalez, J. Ayllon Torresano, A. Cardini, J. Cuevas, J. Del Riego Badas, D. Estrada Acevedo, J. Fernandez Menendez, S. Folgueras, I. Gonzalez Caballero, P. Leguina, M. Obeso Menendez, E. Palencia Cortezon, J. Prado Pico, A. Soto Rodríguez, P. Vischia

Instituto de Física de Cantabria (IFCA), CSIC-Universidad de Cantabria, Santander, Spain
S. Blanco Fernández, I.J. Cabrillo, A. Calderon, J. Duarte Campderros, M. Fernandez, G. Gomez, C. Lasaosa García, R. Lopez Ruiz, C. Martinez Rivero, P. Martinez Ruiz del Arbol, F. Matorras, P. Matorras Cuevas, E. Navarrete Ramos, J. Piedra Gomez, C. Quintana San Emeterio, L. Scodellaro, I. Vila, R. Vilar Cortabitarte, J.M. Vizan Garcia

University of Colombo, Colombo, Sri Lanka
B. Kailasapathy[56], D.D.C. Wickramarathna

University of Ruhuna, Department of Physics, Matara, Sri Lanka
W.G.D. Dharmaratna[57], K. Liyanage, N. Perera

CERN, European Organization for Nuclear Research, Geneva, Switzerland
D. Abbaneo, C. Amendola, R. Ardino, E. Auffray, J. Baechler, D. Barney, J. Bendavid, M. Bianco, A. Bocci, L. Borgonovi, C. Botta, A. Bragagnolo, C.E. Brown, C. Caillol, G. Cerminara, P. Connor, K. Cormier, D. d'Enterria,

A. Dabrowski, A. David, A. De Roeck, M.M. Defranchis, M. Deile, M. Dobson, P.J. Fernández Manteca, B.A. Fontana Santos Alves, E. Fontanesi, W. Funk, A. Gaddi, S. Giani, D. Gigi, K. Gill, F. Glege, M. Glowacki, A. Gruber, J. Hegeman, J.K. Heikkilä, R. Hofsaess, B. Huber, T. James, P. Janot, O. Kaluzinska, O. Karacheban[25], G. Karathanasis, S. Laurila, P. Lecoq, E. Leutgeb, C. Lourenço, A.-M. Lyon, M. Magherini, L. Malgeri, M. Mannelli, A. Mehta, F. Meijers, J.A. Merlin, S. Mersi, E. Meschi, M. Migliorini, F. Monti, F. Moortgat, M. Mulders, M. Musich, I. Neutelings, S. Orfanelli, F. Pantaleo, M. Pari, G. Petrucciani, A. Pfeiffer, M. Pierini, M. Pitt, H. Qu, D. Rabady, A. Reimers, B. Ribeiro Lopes, F. Riti, P. Rosado, M. Rovere, H. Sakulin, R. Salvatico, S. Sanchez Cruz, S. Scarfi, M. Selvaggi, K. Shchelina, P. Silva, P. Sphicas[58], A.G. Stahl Leiton, A. Steen, S. Summers, D. Treille, P. Tropea, E. Vernazza, J. Wanczyk[59], S. Wuchterl, M. Zarucki, P. Zehetner, P. Zejdl, G. Zevi Della Porta

PSI Center for Neutron and Muon Sciences, Villigen, Switzerland
T. Bevilacqua[60], L. Caminada[60], W. Erdmann, R. Horisberger, Q. Ingram, H.C. Kaestli, D. Kotlinski, C. Lange, U. Langenegger, A. Nigamova, L. Noehte[60], T. Rohe, A. Samalan

ETH Zurich - Institute for Particle Physics and Astrophysics (IPA), Zurich, Switzerland
T.K. Aarrestad, M. Backhaus, G. Bonomelli, C. Cazzaniga, K. Datta, P. De Bryas Dexmiers D'Archiacchiac[59], A. De Cosa, G. Dissertori, M. Dittmar, M. Donegà, F. Glessgen, C. Grab, N. Härringer, T.G. Harte, W. Lustermann, M. Malucchi, R.A. Manzoni, L. Marchese, A. Mascellani[59], F. Nessi-Tedaldi, F. Pauss, B. Ristic, R. Seidita, J. Steggemann[59], A. Tarabini, D. Valsecchi, R. Wallny

Universität Zürich, Zurich, Switzerland
C. Amsler[61], P. Bärtschi, F. Bilandzija, M.F. Canelli, G. Celotto, V. Guglielmi, A. Jofrehei, B. Kilminster, T.H. Kwok, S. Leontsinis, V. Lukashenko, A. Macchiolo, F. Meng, M. Missiroli, J. Motta, P. Robmann, E. Shokr, F. Stäger, R. Tramontano, P. Viscone

National Central University, Chung-Li, Taiwan
D. Bhowmik, C.M. Kuo, P.K. Rout, S. Taj, P.C. Tiwari[36]

National Taiwan University (NTU), Taipei, Taiwan
L. Ceard, K.F. Chen, Z.g. Chen, A. De Iorio, W.-S. Hou, T.h. Hsu, Y.w. Kao, S. Karmakar, G. Kole, Y.y. Li, R.-S. Lu, E. Paganis, X.f. Su, J. Thomas-Wilsker, L.s. Tsai, D. Tsionou, H.y. Wu, E. Yazgan

High Energy Physics Research Unit, Department of Physics, Faculty of Science, Chulalongkorn University, Bangkok, Thailand
C. Asawatangtrakuldee, N. Srimanobhas

Tunis El Manar University, Tunis, Tunisia
Y. Maghrbi

Çukurova University, Physics Department, Science and Art Faculty, Adana, Turkey
D. Agyel, F. Dolek, I. Dumanoglu[62], Y. Guler[63], E. Gurpinar Guler[63], C. Isik, O. Kara[64], A. Kayis Topaksu, Y. Komurcu, G. Onengut, K. Ozdemir[65], B. Tali[66], U.G. Tok, E. Uslan, I.S. Zorbakir

Hacettepe University, Ankara, Turkey

S. Sen

Middle East Technical University, Physics Department, Ankara, Turkey
M. Yalvac[67]

Bogazici University, Istanbul, Turkey
B. Akgun, I.O. Atakisi[68], E. Gülmez, M. Kaya[69], O. Kaya[70], M.A. Sarkisla[71], S. Tekten[72]

Istanbul Technical University, Istanbul, Turkey
D. Boncukcu, A. Cakir, K. Cankocak[62,73]

Istanbul University, Istanbul, Turkey
B. Hacisahinoglu, I. Hos[74], B. Kaynak, S. Ozkorucuklu, O. Potok, H. Sert, C. Simsek, C. Zorbilmez

Yildiz Technical University, Istanbul, Turkey
S. Cerci, C. Dozen[75], B. Isildak, E. Simsek, D. Sunar Cerci, T. Yetkin[75]

Institute for Scintillation Materials of National Academy of Science of Ukraine, Kharkiv, Ukraine
A. Boyaryntsev, O. Dadazhanova, B. Grynyov

National Science Centre, Kharkiv Institute of Physics and Technology, Kharkiv, Ukraine
L. Levchuk

University of Bristol, Bristol, United Kingdom
J.J. Brooke, A. Bundock, F. Bury, E. Clement, D. Cussans, D. Dharmender, H. Flacher, J. Goldstein, H.F. Heath, M.-L. Holmberg, L. Kreczko, S. Paramesvaran, L. Robertshaw, M.S. Sanjrani[39], J. Segal, V.J. Smith

Rutherford Appleton Laboratory, Didcot, United Kingdom
A.H. Ball, K.W. Bell, A. Belyaev[76], C. Brew, R.M. Brown, D.J.A. Cockerill, A. Elliot, K.V. Ellis, J. Gajownik, K. Harder, S. Harper, J. Linacre, K. Manolopoulos, M. Moallemi, D.M. Newbold, E. Olaiya, D. Petyt, T. Reis, A.R. Sahasransu, G. Salvi, T. Schuh, C.H. Shepherd-Themistocleous, I.R. Tomalin, K.C. Whalen, T. Williams

Imperial College, London, United Kingdom
I. Andreou, R. Bainbridge, P. Bloch, O. Buchmuller, C.A. Carrillo Montoya, D. Colling, I. Das, P. Dauncey, G. Davies, M. Della Negra, S. Fayer, G. Fedi, G. Hall, H.R. Hoorani, A. Howard, G. Iles, C.R. Knight, P. Krueper, J. Langford, K.H. Law, J. León Holgado, L. Lyons, A.-M. Magnan, B. Maier, S. Mallios, A. Mastronikolis, M. Mieskolainen, J. Nash[77], M. Pesaresi, P.B. Pradeep, B.C. Radburn-Smith, A. Richards, A. Rose, L. Russell, K. Savva, C. Seez, R. Shukla, A. Tapper, K. Uchida, G.P. Uttley, T. Virdee[27], M. Vojinovic, N. Wardle, D. Winterbottom

Brunel University, Uxbridge, United Kingdom
J.E. Cole, A. Khan, P. Kyberd, I.D. Reid

Baylor University, Waco, Texas, USA
S. Abdullin, A. Brinkerhoff, E. Collins, M.R. Darwish, J. Dittmann, K. Hatakeyama, V. Hegde, J. Hiltbrand, B. McMaster, J. Samudio, S. Sawant, C. Sutantawibul, J. Wilson

Bethel University, St. Paul, Minnesota, USA
J.M. Hogan

Catholic University of America, Washington, DC, USA
R. Bartek, A. Dominguez, S. Raj, B. Sahu[35], A.E. Simsek, S.S. Yu

The University of Alabama, Tuscaloosa, Alabama, USA
B. Bam, A. Buchot Perraguin, S. Campbell, R. Chudasama, S.I. Cooper, C. Crovella, G. Fidalgo, S.V. Gleyzer, A. Khukhunaishvili, K. Matchev, E. Pearson, P. Rumerio[78], E. Usai, R. Yi

Boston University, Boston, Massachusetts, USA
S. Cholak, G. De Castro, Z. Demiragli, C. Erice, C. Fangmeier, C. Fernandez Madrazo, J. Fulcher, F. Golf, S. Jeon, J. O'Cain, I. Reed, J. Rohlf, K. Salyer, D. Sperka, D. Spitzbart, I. Suarez, A. Tsatsos, E. Wurtz, A.G. Zecchinelli

Brown University, Providence, Rhode Island, USA
G. Barone, G. Benelli, D. Cutts, S. Ellis, L. Gouskos, M. Hadley, U. Heintz, K.W. Ho, T. Kwon, L. Lambrecht, G. Landsberg, K.T. Lau, J. Luo, S. Mondal, J. Roloff, T. Russell, S. Sagir[79], X. Shen, M. Stamenkovic, N. Venkatasubramanian

University of California, Davis, Davis, California, USA
S. Abbott, S. Baradia, B. Barton, R. Breedon, H. Cai, M. Calderon De La Barca Sanchez, E. Cannaert, M. Chertok, M. Citron, J. Conway, P.T. Cox, F. Eble, R. Erbacher, O. Kukral, G. Mocellin, S. Ostrom, I. Salazar Segovia, J.S. Tafoya Vargas, W. Wei, S. Yoo

University of California, Los Angeles, California, USA
K. Adamidis, M. Bachtis, D. Campos, R. Cousins, S. Crossley, G. Flores Avila, J. Hauser, M. Ignatenko, M.A. Iqbal, T. Lam, Y.f. Lo, E. Manca, A. Nunez Del Prado, D. Saltzberg, V. Valuev

University of California, Riverside, Riverside, California, USA
R. Clare, J.W. Gary, G. Hanson

University of California, San Diego, La Jolla, California, USA
A. Aportela, A. Arora, J.G. Branson, S. Cittolin, S. Cooperstein, B. D'Anzi, D. Diaz, J. Duarte, L. Giannini, Y. Gu, J. Guiang, V. Krutelyov, R. Lee, J. Letts, H. Li, M. Masciovecchio, F. Mokhtar, S. Mukherjee, M. Pieri, D. Primosch, M. Quinnan, V. Sharma, M. Tadel, E. Vourliotis, F. Würthwein, A. Yagil, Z. Zhao

University of California, Santa Barbara - Department of Physics, Santa Barbara, California, USA
A. Barzdukas, L. Brennan, C. Campagnari, S. Carron Montero[80], K. Downham, C. Grieco, M.M. Hussain, J. Incandela, M.W.K. Lai, A.J. Li, P. Masterson, J. Richman, S.N. Santpur, R. Schmitz, D. Stuart, T.Á. Vámi, X. Yan, D. Zhang

California Institute of Technology, Pasadena, California, USA
A. Albert, S. Bhattacharya, A. Bornheim, O. Cerri, R. Kansal, J. Mao, H.B. Newman, G. Reales Gutiérrez, T. Sievert, M. Spiropulu, J.R. Vlimant, R.A. Wynne, S. Xie

Carnegie Mellon University, Pittsburgh, Pennsylvania, USA
J. Alison, S. An, M. Cremonesi, V. Dutta, E.Y. Ertorer, T. Ferguson, T.A. Gómez Es-

pinosa, A. Harilal, A. Kallil Tharayil, M. Kanemura, C. Liu, M. Marchegiani, P. Meiring, S. Murthy, P. Palit, K. Park, M. Paulini, A. Roberts, A. Sanchez, W. Terrill

University of Colorado Boulder, Boulder, Colorado, USA
J.P. Cumalat, W.T. Ford, A. Hart, S. Kwan, J. Pearkes, C. Savard, N. Schonbeck, K. Stenson, K.A. Ulmer, S.R. Wagner, N. Zipper, D. Zuolo

Cornell University, Ithaca, New York, USA
J. Alexander, X. Chen, J. Dickinson, A. Duquette, J. Fan, X. Fan, J. Grassi, S. Hogan, P. Kotamnives, J. Monroy, G. Niendorf, M. Oshiro, J.R. Patterson, A. Ryd, J. Thom, P. Wittich, R. Zou, L. Zygala

Fermi National Accelerator Laboratory, Batavia, Illinois, USA
M. Albrow, M. Alyari, O. Amram, G. Apollinari, A. Apresyan, L.A.T. Bauerdick, D. Berry, J. Berryhill, P.C. Bhat, K. Burkett, J.N. Butler, A. Canepa, G.B. Cerati, H.W.K. Cheung, F. Chlebana, C. Cosby, G. Cummings, I. Dutta, V.D. Elvira, J. Freeman, A. Gandrakota, Z. Gecse, L. Gray, D. Green, A. Grummer, S. Grünendahl, D. Guerrero, O. Gutsche, R.M. Harris, J. Hirschauer, V. Innocente, B. Jayatilaka, S. Jindariani, M. Johnson, U. Joshi, B. Klima, S. Lammel, C. Lee, D. Lincoln, R. Lipton, T. Liu, K. Maeshima, D. Mason, P. McBride, P. Merkel, S. Mrenna, S. Nahn, J. Ngadiuba, D. Noonan, S. Norberg, V. Papadimitriou, N. Pastika, K. Pedro, C. Pena[81], C.E. Perez Lara, V. Perovic, F. Ravera, A. Reinsvold Hall[82], L. Ristori, M. Safdari, E. Sexton-Kennedy, E. Smith, N. Smith, A. Soha, L. Spiegel, S. Stoynev, J. Strait, L. Taylor, S. Tkaczyk, N.V. Tran, L. Uplegger, E.W. Vaandering, C. Wang, I. Zoi

University of Florida, Gainesville, Florida, USA
C. Aruta, P. Avery, D. Bourilkov, P. Chang, V. Cherepanov, R.D. Field, C. Huh, E. Koenig, M. Kolosova, J. Konigsberg, A. Korytov, G. Mitselmakher, K. Mohrman, A. Muthirakalayil Madhu, N. Rawal, S. Rosenzweig, V. Sulimov, Y. Takahashi, J. Wang

Florida State University, Tallahassee, Florida, USA
T. Adams, A. Al Kadhim, A. Askew, S. Bower, R. Goff, R. Hashmi, A. Hassani, R.S. Kim, T. Kolberg, G. Martinez, M. Mazza, H. Prosper, P.R. Prova, R. Yohay

Florida Institute of Technology, Melbourne, Florida, USA
B. Alsufyani, S. Butalla, S. Das, M. Hohlmann, M. Lavinsky, E. Yanes

University of Illinois Chicago, Chicago, Illinois, USA
M.R. Adams, N. Barnett, A. Baty, C. Bennett, R. Cavanaugh, R. Escobar Franco, O. Evdokimov, C.E. Gerber, H. Gupta, M. Hawksworth, A. Hingrajiya, D.J. Hofman, Z. Huang, J.h. Lee, C. Mills, S. Nanda, G. Nigmatkulov, B. Ozek, T. Phan, D. Pilipovic, R. Pradhan, E. Prifti, P. Roy, T. Roy, D. Shekar, N. Singh, A. Thielen, M.B. Tonjes, N. Varelas, M.A. Wadud, J. Yoo

The University of Iowa, Iowa City, Iowa, USA
M. Alhusseini, D. Blend, K. Dilsiz[83], O.K. Köseyan, A. Mestvirishvili[84], O. Neogi, H. Ogul[85], Y. Onel, A. Penzo, C. Snyder, E. Tiras[86]

Johns Hopkins University, Baltimore, Maryland, USA
B. Blumenfeld, J. Davis, A.V. Gritsan, L. Kang, S. Kyriacou, P. Maksimovic, M. Roguljic, S. Sekhar, M.V. Srivastav, M. Swartz

The University of Kansas, Lawrence, Kansas, USA
A. Abreu, L.F. Alcerro Alcerro, J. Anguiano, S. Arteaga Escatel, P. Baringer, A. Bean, R. Bhattacharya, Z. Flowers, D. Grove, J. King, G. Krintiras, M. Lazarovits, C. Le Mahieu, J. Marquez, M. Murray, M. Nickel, S. Popescu[87], C. Rogan, C. Royon, S. Rudrabhatla, S. Sanders, C. Smith, G. Wilson

Kansas State University, Manhattan, Kansas, USA
B. Allmond, N. Islam, A. Ivanov, K. Kaadze, Y. Maravin, J. Natoli, G.G. Reddy, D. Roy, G. Sorrentino

University of Maryland, College Park, Maryland, USA
A. Baden, A. Belloni, J. Bistany-riebman, S.C. Eno, N.J. Hadley, S. Jabeen, R.G. Kellogg, T. Koeth, B. Kronheim, S. Lascio, P. Major, A.C. Mignerey, C. Palmer, C. Papageorgakis, M.M. Paranjpe, E. Popova[88], A. Shevelev, L. Zhang

Massachusetts Institute of Technology, Cambridge, Massachusetts, USA
C. Baldenegro Barrera, H. Bossi, S. Bright-Thonney, I.A. Cali, Y.c. Chen, P.c. Chou, M. D'Alfonso, J. Eysermans, C. Freer, G. Gomez-Ceballos, M. Goncharov, G. Grosso, P. Harris, D. Hoang, G.M. Innocenti, K. Ivanov, D. Kovalskyi, J. Krupa, L. Lavezzo, Y.-J. Lee, K. Long, C. Mcginn, A. Novak, M.I. Park, C. Paus, C. Reissel, C. Roland, G. Roland, S. Rothman, T.a. Sheng, G.S.F. Stephans, D. Walter, J. Wang, Z. Wang, B. Wyslouch, T. J. Yang

University of Minnesota, Minneapolis, Minnesota, USA
A. Alpana, B. Crossman, W.J. Jackson, C. Kapsiak, M. Krohn, D. Mahon, J. Mans, B. Marzocchi, R. Rusack, O. Sancar, R. Saradhy, N. Strobbe

University of Nebraska-Lincoln, Lincoln, Nebraska, USA
K. Bloom, D.R. Claes, G. Haza, J. Hossain, C. Joo, I. Kravchenko, K.H.M. Kwok, A. Rohilla, J.E. Siado, W. Tabb, A. Vagnerini, A. Wightman, F. Yan

State University of New York at Buffalo, Buffalo, New York, USA
H. Bandyopadhyay, L. Hay, H.w. Hsia, I. Iashvili, A. Kalogeropoulos, A. Kharchilava, A. Mandal, M. Morris, D. Nguyen, S. Rappoccio, H. Rejeb Sfar, A. Williams, D. Yu

Northeastern University, Boston, Massachusetts, USA
A. Aarif, G. Alverson, E. Barberis, J. Bonilla, B. Bylsma, M. Campana, J. Dervan, Y. Haddad, Y. Han, I. Israr, A. Krishna, M. Lu, N. Manganelli, R. Mccarthy, D.M. Morse, T. Orimoto, L. Skinnari, C.S. Thoreson, E. Tsai, D. Wood

Northwestern University, Evanston, Illinois, USA
S. Dittmer, K.A. Hahn, M. Mcginnis, Y. Miao, D.G. Monk, M.H. Schmitt, A. Taliercio, M. Velasco, J. Wang

University of Notre Dame, Notre Dame, Indiana, USA
G. Agarwal, R. Band, R. Bucci, S. Castells, A. Das, A. Datta, A. Ehnis, R. Goldouzian, M. Hildreth, K. Hurtado Anampa, T. Ivanov, C. Jessop, A. Karneyeu, K. Lannon, J. Lawrence, N. Loukas, L. Lutton, J. Mariano, N. Marinelli, T. McCauley, C. Mcgrady, C. Moore, Y. Musienko[21], H. Nelson, M. Osherson, A. Piccinelli, R. Ruchti, A. Townsend, Y. Wan, M. Wayne, H. Yockey

The Ohio State University, Columbus, Ohio, USA

M. Carrigan, R. De Los Santos, L.S. Durkin, C. Hill, M. Joyce, D.A. Wenzl, B.L. Winer, B. R. Yates

Princeton University, Princeton, New Jersey, USA
H. Bouchamaoui, G. Dezoort, P. Elmer, A. Frankenthal, M. Galli, B. Greenberg, N. Haubrich, K. Kennedy, G. Kopp, Y. Lai, D. Lange, A. Loeliger, D. Marlow, I. Ojalvo, J. Olsen, F. Simpson, D. Stickland, C. Tully

University of Puerto Rico, Mayaguez, Puerto Rico, USA
S. Malik, R. Sharma

Purdue University, West Lafayette, Indiana, USA
S. Chandra, A. Gu, L. Gutay, M. Huwiler, M. Jones, A.W. Jung, D. Kondratyev, J. Li, M. Liu, G. Negro, N. Neumeister, G. Paspalaki, S. Piperov, N.R. Saha, J.F. Schulte, F. Wang, A. Wildridge, W. Xie, Y. Yao, Y. Zhong

Purdue University Northwest, Hammond, Indiana, USA
N. Parashar, A. Pathak, E. Shumka

Rice University, Houston, Texas, USA
D. Acosta, A. Agrawal, C. Arbour, T. Carnahan, P. Das, K.M. Ecklund, F.J.M. Geurts, T. Huang, I. Krommydas, N. Lewis, W. Li, J. Lin, O. Miguel Colin, B.P. Padley, R. Redjimi, J. Rotter, C. Vico Villalba, M. Wulansatiti, E. Yigitbasi, Y. Zhang

University of Rochester, Rochester, New York, USA
O. Bessidskaia Bylund, A. Bodek, P. de Barbaro[†], R. Demina, A. Garcia-Bellido, H.S. Hare, O. Hindrichs, N. Parmar, P. Parygin[88], H. Seo, R. Taus

Rutgers, The State University of New Jersey, Piscataway, New Jersey, USA
B. Chiarito, J.P. Chou, S.V. Clark, S. Donnelly, D. Gadkari, Y. Gershtein, E. Halkiadakis, C. Houghton, D. Jaroslawski, A. Kobert, I. Laflotte, A. Lath, J. Martins, M. Perez Prada, B. Rand, J. Reichert, P. Saha, S. Salur, S. Schnetzer, S. Somalwar, R. Stone, S.A. Thayil, S. Thomas, J. Vora

University of Tennessee, Knoxville, Tennessee, USA
D. Ally, A.G. Delannoy, S. Fiorendi, J. Harris, T. Holmes, A.R. Kanuganti, N. Karunarathna, J. Lawless, L. Lee, E. Nibigira, B. Skipworth, S. Spanier

Texas A&M University, College Station, Texas, USA
D. Aebi, M. Ahmad, T. Akhter, K. Androsov, A. Basnet, A. Bolshov, O. Bouhali[89], A. Cagnotta, V. D'Amante, R. Eusebi, P. Flanagan, J. Gilmore, Y. Guo, T. Kamon, S. Luo, R. Mueller, A. Safonov

Texas Tech University, Lubbock, Texas, USA
N. Akchurin, J. Damgov, Y. Feng, N. Gogate, W. Jin, Y. Kazhykarim, K. Lamichhane, S.W. Lee, C. Madrid, A. Mankel, T. Peltola, I. Volobouev

Vanderbilt University, Nashville, Tennessee, USA
E. Appelt, Y. Chen, S. Greene, A. Gurrola, W. Johns, R. Kunnawalkam Elayavalli, A. Melo, D. Rathjens, F. Romeo, P. Sheldon, S. Tuo, J. Velkovska, J. Viinikainen, J. Zhang

University of Virginia, Charlottesville, Virginia, USA
B. Cardwell, H. Chung, B. Cox, J. Hakala, G. Hamilton Ilha Machado, R. Hirosky,

M. Jose, A. Ledovskoy, C. Mantilla, C. Neu, C. Ramón Álvarez, Z. Wu

Wayne State University, Detroit, Michigan, USA
S. Bhattacharya, P.E. Karchin

University of Wisconsin - Madison, Madison, Wisconsin, USA
A. Aravind, S. Banerjee, K. Black, T. Bose, E. Chavez, S. Dasu, P. Everaerts, C. Galloni, H. He, M. Herndon, A. Herve, C.K. Koraka, S. Lomte, R. Loveless, A. Mallampalli, A. Mohammadi, S. Mondal, T. Nelson, G. Parida, L. Pétré, D. Pinna, A. Savin, V. Shang, V. Sharma, W.H. Smith, D. Teague, H.F. Tsoi, W. Vetens, A. Warden

Authors affiliated with an international laboratory covered by a cooperation agreement with CERN
S. Afanasiev, V. Alexakhin, Yu. Andreev, T. Aushev, D. Budkouski, R. Chistov, M. Danilov, T. Dimova, A. Ershov, S. Gninenko, I. Gorbunov, A. Gribushin, A. Kamenev, V. Karjavine, M. Kirsanov, V. Klyukhin, O. Kodolova[90], V. Korenkov, I. Korsakov, A. Kozyrev, N. Krasnikov, A. Lanev, A. Malakhov, V. Matveev, A. Nikitenko[91,90], V. Palichik, V. Perelygin, S. Petrushanko, O. Radchenko, M. Savina, V. Shalaev, S. Shmatov, S. Shulha, Y. Skovpen, K. Slizhevskiy, V. Smirnov, O. Teryaev, I. Tlisova, A. Toropin, N. Voytishin, A. Zarubin, I. Zhizhin

Authors affiliated with an institute formerly covered by a cooperation agreement with CERN
L. Dudko, V. Kim[21], V. Murzin, V. Oreshkin, D. Sosnov, E. Boos, V. Bunichev, M. Dubinin[81], V. Savrin, A. Snigirev

†: Deceased
[1]Also at Yerevan State University, Yerevan, Armenia
[2]Also at TU Wien, Vienna, Austria
[3]Also at Ghent University, Ghent, Belgium
[4]Also at FACAMP - Faculdades de Campinas, Sao Paulo, Brazil
[5]Also at Universidade Estadual de Campinas, Campinas, Brazil
[6]Also at Federal University of Rio Grande do Sul, Porto Alegre, Brazil
[7]Also at The University of the State of Amazonas, Manaus, Brazil
[8]Also at University of Chinese Academy of Sciences, Beijing, China
[9]Also at University of Chinese Academy of Sciences, Beijing, China
[10]Also at School of Physics, Zhengzhou University, Zhengzhou, China
[11]Now at Henan Normal University, Xinxiang, China
[12]Also at University of Shanghai for Science and Technology, Shanghai, China
[13]Also at The University of Iowa, Iowa City, Iowa, USA
[14]Also at Nanjing Normal University, Nanjing, China
[15]Also at Center for High Energy Physics, Peking University, Beijing, China
[16]Also at Zewail City of Science and Technology, Zewail, Egypt
[17]Also at British University in Egypt, Cairo, Egypt
[18]Now at Ain Shams University, Cairo, Egypt
[19]Also at Purdue University, West Lafayette, Indiana, USA
[20]Also at Université de Haute Alsace, Mulhouse, France
[21]Also at an institute formerly covered by a cooperation agreement with CERN
[22]Also at University of Hamburg, Hamburg, Germany
[23]Also at RWTH Aachen University, III. Physikalisches Institut A, Aachen, Germany
[24]Also at Bergische University Wuppertal (BUW), Wuppertal, Germany

[25]Also at Brandenburg University of Technology, Cottbus, Germany
[26]Also at Forschungszentrum Jülich, Juelich, Germany
[27]Also at CERN, European Organization for Nuclear Research, Geneva, Switzerland
[28]Also at HUN-REN ATOMKI - Institute of Nuclear Research, Debrecen, Hungary
[29]Now at Universitatea Babes-Bolyai - Facultatea de Fizica, Cluj-Napoca, Romania
[30]Also at MTA-ELTE Lendület CMS Particle and Nuclear Physics Group, Eötvös Loránd University, Budapest, Hungary
[31]Also at HUN-REN Wigner Research Centre for Physics, Budapest, Hungary
[32]Also at Physics Department, Faculty of Science, Assiut University, Assiut, Egypt
[33]Also at The University of Kansas, Lawrence, Kansas, USA
[34]Also at Punjab Agricultural University, Ludhiana, India
[35]Also at University of Hyderabad, Hyderabad, India
[36]Also at Indian Institute of Science (IISc), Bangalore, India
[37]Also at University of Visva-Bharati, Santiniketan, India
[38]Also at Institute of Physics, Bhubaneswar, India
[39]Also at Deutsches Elektronen-Synchrotron, Hamburg, Germany
[40]Also at Isfahan University of Technology, Isfahan, Iran
[41]Also at Sharif University of Technology, Tehran, Iran
[42]Also at Department of Physics, University of Science and Technology of Mazandaran, Behshahr, Iran
[43]Also at Department of Physics, Faculty of Science, Arak University, ARAK, Iran
[44]Also at Helwan University, Cairo, Egypt
[45]Also at Italian National Agency for New Technologies, Energy and Sustainable Economic Development, Bologna, Italy
[46]Also at Centro Siciliano di Fisica Nucleare e di Struttura Della Materia, Catania, Italy
[47]Also at James Madison University, Harrisonburg, Maryland, USA
[48]Also at Università degli Studi Guglielmo Marconi, Roma, Italy
[49]Also at Scuola Superiore Meridionale, Università di Napoli 'Federico II', Napoli, Italy
[50]Also at Fermi National Accelerator Laboratory, Batavia, Illinois, USA
[51]Also at Lulea University of Technology, Lulea, Sweden
[52]Also at Consiglio Nazionale delle Ricerche - Istituto Officina dei Materiali, Perugia, Italy
[53]Also at UPES - University of Petroleum and Energy Studies, Dehradun, India
[54]Also at Institut de Physique des 2 Infinis de Lyon (IP2I), Villeurbanne, France
[55]Also at Department of Applied Physics, Faculty of Science and Technology, Universiti Kebangsaan Malaysia, Bangi, Malaysia
[56]Also at Trincomalee Campus, Eastern University, Sri Lanka, Nilaveli, Sri Lanka
[57]Also at Saegis Campus, Nugegoda, Sri Lanka
[58]Also at National and Kapodistrian University of Athens, Athens, Greece
[59]Also at Ecole Polytechnique Fédérale Lausanne, Lausanne, Switzerland
[60]Also at Universität Zürich, Zurich, Switzerland
[61]Also at Stefan Meyer Institute for Subatomic Physics, Vienna, Austria
[62]Also at Near East University, Research Center of Experimental Health Science, Mersin, Turkey
[63]Also at Konya Technical University, Konya, Turkey
[64]Also at Istanbul Topkapi University, Istanbul, Turkey
[65]Also at Izmir Bakircay University, Izmir, Turkey
[66]Also at Adiyaman University, Adiyaman, Turkey
[67]Also at Bozok Universitetesi Rektörlügü, Yozgat, Turkey
[68]Also at Istanbul Sabahattin Zaim University, Istanbul, Turkey

[69]Also at Marmara University, Istanbul, Turkey
[70]Also at Milli Savunma University, Istanbul, Turkey
[71]Also at Informatics and Information Security Research Center, Gebze/Kocaeli, Turkey
[72]Also at Kafkas University, Kars, Turkey
[73]Now at Istanbul Okan University, Istanbul, Turkey
[74]Also at Istanbul University - Cerrahpasa, Faculty of Engineering, Istanbul, Turkey
[75]Also at Istinye University, Istanbul, Turkey
[76]Also at School of Physics and Astronomy, University of Southampton, Southampton, United Kingdom
[77]Also at Monash University, Faculty of Science, Clayton, Australia
[78]Also at Università di Torino, Torino, Italy
[79]Also at Karamanoğlu Mehmetbey University, Karaman, Turkey
[80]Also at California Lutheran University, Thousand Oaks, California, USA
[81]Also at California Institute of Technology, Pasadena, California, USA
[82]Also at United States Naval Academy, Annapolis, Maryland, USA
[83]Also at Bingol University, Bingol, Turkey
[84]Also at Georgian Technical University, Tbilisi, Georgia
[85]Also at Sinop University, Sinop, Turkey
[86]Also at Erciyes University, Kayseri, Turkey
[87]Also at Horia Hulubei National Institute of Physics and Nuclear Engineering (IFIN-HH), Bucharest, Romania
[88]Now at another institute formerly covered by a cooperation agreement with CERN
[89]Also at Hamad Bin Khalifa University (HBKU), Doha, Qatar
[90]Also at Yerevan Physics Institute, Yerevan, Armenia
[91]Also at Imperial College, London, United Kingdom